NASA TECHNICAL NOTE

NASA TN D-4179

NASA TN D-4179

NASA TN D-4179
c.1

LOAN COPY: RETURN TO
AFWL (WLIL-2)
KIRTLAND AFB, N MEX

TECH LIBRARY KAFB, NM
0130719

LOW-SUBSONIC FLIGHT AND FORCE INVESTIGATION OF A SUPERSONIC TRANSPORT MODEL WITH A DOUBLE-DELTA WING

by Delma C. Freeman, Jr.

Langley Research Center
Langley Station, Hampton, Va.

NATIONAL AERONAUTICS AND SPACE ADMINISTRATION • WASHINGTON, D. C. • MARCH 1968

TECH LIBRARY KAFB, NM
0130719

NASA TN D-4179

LOW-SUBSONIC FLIGHT AND FORCE INVESTIGATION OF A SUPERSONIC TRANSPORT MODEL WITH A DOUBLE-DELTA WING

By Delma C. Freeman, Jr.

Langley Research Center
Langley Station, Hampton, Va.

Technical Film Supplement L-970 available on request.

NATIONAL AERONAUTICS AND SPACE ADMINISTRATION

For sale by the Clearinghouse for Federal Scientific and Technical Information
Springfield, Virginia 22151 – CFSTI price $3.00

LOW-SUBSONIC FLIGHT AND FORCE INVESTIGATION OF A SUPERSONIC TRANSPORT MODEL WITH A DOUBLE-DELTA WING

By Delma C. Freeman, Jr.
Langley Research Center

SUMMARY

An investigation has been conducted in the Langley full-scale tunnel to determine the low-speed static and dynamic longitudinal and lateral stability characteristics of a 1/20-scale model of a double-delta supersonic commercial air transport configuration.

The results of the investigation showed that the dynamic longitudinal stability and control characteristics of the model were generally satisfactory over the test angle-of-attack range except from about 20° to 25° where neutral or negative static longitudinal stability made flying difficult. The Dutch roll oscillation was well damped throughout most of the test angle-of-attack range but the damping decreased rapidly above an angle of attack of about 20°. The use of a roll-rate damper to provide artificial stabilization in roll generally gave satisfactory Dutch roll characteristics over the test angle-of-attack range. The directional stability was satisfactory at low angles of attack but deteriorated rapidly at the high angles of attack and the model diverged in yaw against full corrective control near an angle of attack of 28°. The lateral control characteristics were satisfactory over the test angle-of-attack range.

INTRODUCTION

For the past few years, the National Aeronautics and Space Administration has been conducting extensive research in support of a supersonic transport program. As part of this general effort the Langley Research Center has conducted an investigation in the Langley full-scale tunnel to determine the low-speed static and dynamic stability characteristics of a 1/20-scale model of a proposed supersonic commercial air transport configuration with a double-delta wing. The double-delta wing has been proposed as a configuration for reducing the large rearward aerodynamic-center shift that occurs when the speed is changed from subsonic to supersonic flight. This effect is realized in this configuration because of the change in aerodynamic loading from the rear delta at low speeds to the forward delta at high speeds.

The investigation consisted of free-flight tests to determine the low-speed dynamic stability and control characteristics of the configuration. In addition, both static and dynamic force tests were made to document the aerodynamic characteristics of the flight-test model, and dynamic longitudinal and lateral stability calculations were made to provide information for correlation with the flight-test results.

SYMBOLS

The longitudinal data are referred to the stability system of axes and the lateral data are referred to the body system of axes (see fig. 1). The origin of the axes was located to correspond to the center-of-gravity position shown in figure 2.

In order to facilitate international usage of data presented, dimensional quantities are presented both in the U.S. Customary Units and in the International System of Units (SI). The equivalent dimensions were determined in each case by using the conversion factors given in reference 1.

b	wing span, ft (m)
$1/C_{1/2}$	inverse cyclic damping
$\bar{c}$	mean aerodynamic chord, ft (m)
e_1	control surface located between inboard nacelle and fuselage (fig. 2)
e_2	control surface located between inboard and outboard nacelles (fig. 2)
e_3	control surface located outboard of outboard nacelle (fig. 2)
F_A	axial force, lb (N)
F_D	drag force, lb (N)
F_L	lift force, lb (N)
F_N	normal force, lb (N)
F_Y	lateral force, lb (N)
f	frequency of oscillations, cps

I_X	moment of inertia about longitudinal body axis, slug-ft^2 (kg-m^2)
I_Z	moment of inertia about normal body axis, slug-ft^2 (kg-m^2)
k	reduced-frequency parameter, $\omega b/2V$ or $\omega \bar{c}/2V$
L/D	lift-drag ratio
M_X	rolling moment, ft-lb (N-m)
M_Y	pitching moment, ft-lb (N-m)
M_Z	yawing moment, ft-lb (N-m)
m	mass, slugs (kg)
P	period, sec
p	rolling velocity, rad/sec
$\dot{p}$	rolling acceleration, dp/dt, rad/sec^2
q	pitching velocity, rad/sec
$\dot{q}$	pitching acceleration, rad/sec^2
q_∞	dynamic pressure, lb/ft^2 (N/m^2)
r	yawing velocity, rad/sec
$\dot{r}$	yawing acceleration, dr/dt, rad/sec^2
S	wing area, ft^2 (m^2)
t	time, sec
$t_{1/2}$	time to damp to half-amplitude, sec
V	free-stream velocity, ft/sec (m/sec)

$v_e = V\sqrt{\sigma} \sin \beta \approx V\sqrt{\sigma}\beta$

$\left|\frac{\phi}{v_e}\right|$ ratio of bank-angle amplitude to equivalent side-velocity amplitude for oscillatory mode, $\left|\frac{\phi}{\beta}\right|\frac{57.3}{V\sqrt{\sigma}}, \frac{\text{deg}}{\text{ft/sec}} \left(\frac{\text{deg}}{\text{m/sec}}\right)$

X,Y,Z body reference axes

X_s,Y_s,Z_s stability reference axes

α angle of attack, deg or rad

$\dot{\alpha}$ rate of change of angle of attack, rad/sec

β angle of sideslip, deg or rad

$\dot{\beta}$ rate of change of angle of sideslip, rad/sec

δ_a total aileron deflection, $\delta_{e,L} - \delta_{e,R}$, deg

δ_e elevator deflection, positive when trailing edge is down (subscripts 1, 2, and 3 indicate particular control surface, see fig. 2), deg

$\delta_{e,L}$ left elevon deflection, positive when trailing edge is down, deg

$\delta_{e,R}$ right elevon deflection, positive when trailing edge is down, deg

δ_n leading-edge flap deflection, negative when leading edge is down, deg

δ_r rudder deflection, positive when trailing edge is deflected to left, deg

μ relative-density factor, $m/\rho Sb$

ρ air density, slug/ft^3 (kg/m^3)

σ ratio of air density at altitude to that at sea level

ϕ angle of roll, deg or rad

$\dot{\phi}$ rate of change of angle of roll, deg/sec or rad/sec

ψ angle of yaw, deg or rad

ω angular velocity, $2\pi f$, rad/sec

C_A axial-force coefficient, $F_A/q_\infty S$

C_D drag coefficient, $F_D/q_\infty S$

C_L lift coefficient, $F_L/q_\infty S$

C_l rolling-moment coefficient, $M_X/q_\infty Sb$

ΔC_l incremental rolling-moment coefficient

$C_{l_\beta} = \frac{\partial C_l}{\partial \beta}$, per deg or per rad

C_m pitching-moment coefficient, $M_Y/q_\infty S\bar{c}$

C_N normal-force coefficient, $F_N/q_\infty S$

C_n yawing-moment coefficient, $M_Z/q_\infty Sb$

ΔC_n incremental yawing-moment coefficient

$C_{n_\beta} = \frac{\partial C_n}{\partial \beta}$, per deg or per rad

$C_{n_{\beta,\text{dynamic}}} = C_{n_\beta} - \frac{I_Z}{I_X} C_{l_\beta} \sin \alpha$

C_Y side-force coefficient, $F_Y/q_\infty S$

ΔC_Y incremental side-force coefficient

$C_{Y_\beta} = \frac{\partial C_Y}{\partial \beta}$, per deg or per rad

$$C_{l_p} = \frac{\partial C_l}{\partial \frac{pb}{2V}} \qquad C_{n_p} = \frac{\partial C_n}{\partial \frac{pb}{2V}} \qquad C_{Y_p} = \frac{\partial C_Y}{\partial \frac{pb}{2V}}$$

$$C_{l_{\dot{p}}} = \frac{\partial C_l}{\partial \frac{\dot{p}b^2}{4V^2}} \qquad C_{n_{\dot{p}}} = \frac{\partial C_n}{\partial \frac{\dot{p}b^2}{4V^2}} \qquad C_{Y_{\dot{p}}} = \frac{\partial C_Y}{\partial \frac{\dot{p}b^2}{4V^2}}$$

$$C_{l_r} = \frac{\partial C_l}{\partial \frac{rb}{2V}} \qquad C_{n_r} = \frac{\partial C_n}{\partial \frac{rb}{2V}} \qquad C_{Y_r} = \frac{\partial C_Y}{\partial \frac{rb}{2V}}$$

$$C_{l_{\dot{r}}} = \frac{\partial C_l}{\partial \frac{\dot{r}b^2}{4V^2}} \qquad C_{n_{\dot{r}}} = \frac{\partial C_n}{\partial \frac{\dot{r}b^2}{4V^2}} \qquad C_{Y_{\dot{r}}} = \frac{\partial C_Y}{\partial \frac{\dot{r}b^2}{4V^2}}$$

$$C_{l_{\dot{\beta}}} = \frac{\partial C_l}{\partial \frac{\dot{\beta}b}{2V}} \qquad C_{n_{\dot{\beta}}} = \frac{\partial C_n}{\partial \frac{\dot{\beta}b}{2V}} \qquad C_{Y_{\dot{\beta}}} = \frac{\partial C_Y}{\partial \frac{\dot{\beta}b}{2V}}$$

$$C_{m_\alpha} = \frac{\partial C_m}{\partial \alpha} \qquad C_{A_\alpha} = \frac{\partial C_A}{\partial \alpha} \qquad C_{N_\alpha} = \frac{\partial C_N}{\partial \alpha}$$

$$C_{m_{\dot{\alpha}}} = \frac{\partial C_m}{\partial \frac{\dot{\alpha}\bar{c}}{2V}} \qquad C_{A_{\dot{\alpha}}} = \frac{\partial C_A}{\partial \frac{\dot{\alpha}\bar{c}}{2V}} \qquad C_{N_{\dot{\alpha}}} = \frac{\partial C_N}{\partial \frac{\dot{\alpha}\bar{c}}{2V}}$$

$$C_{m_q} = \frac{\partial C_m}{\partial \frac{q\bar{c}}{2V}} \qquad C_{A_q} = \frac{\partial C_A}{\partial \frac{q\bar{c}}{2V}} \qquad C_{N_q} = \frac{\partial C_N}{\partial \frac{q\bar{c}}{2V}}$$

$$C_{m_{\dot{q}}} = \frac{\partial C_m}{\partial \frac{\dot{q}\bar{c}^2}{4V^2}} \qquad C_{A_{\dot{q}}} = \frac{\partial C_A}{\partial \frac{\dot{q}\bar{c}^2}{4V^2}} \qquad C_{N_{\dot{q}}} = \frac{\partial C_N}{\partial \frac{\dot{q}\bar{c}^2}{4V^2}}$$

APPARATUS AND MODEL

A drawing of the 1/20-scale model used in the investigation is presented in figure 2, and the mass and dimensional characteristics of the model are presented in table I. The model had a double-delta wing with 83° sweep on the forward delta and 65° sweep on the main wing. It had a single vertical tail and had four nacelles located under the wing. The main wing was equipped with full-span leading-edge flaps and trailing-edge control surfaces. Longitudinal trim and control were obtained by symmetrical deflection of all the wing trailing-edge control surfaces (elevons e_1, e_2, and e_3) during most of the flights. Lateral directional control was obtained by differential deflection of the elevons in combination with the rudder. For a few flights, various segments of the elevons were deflected individually to provide additional control information.

The flight tests of the model were made in the Langley full-scale tunnel, and a sketch of the test equipment and setup is given in figure 3. A photograph of the model flying in the tunnel is presented in figure 4(a). All force tests were made in the Langley full-scale tunnel with a sting support system and internal strain-gage balances. A photograph of the model mounted for static force tests is shown in figure 4(b). The longitudinal

oscillation tests were made on an apparatus similar to the one described in reference 2. The lateral oscillation tests were made on an apparatus similar to the one described in reference 3, except that an automatic readout system was employed.

TESTS

Flight Tests

The flight tests were made to determine the dynamic stability and control characteristics and the general flight behavior of the model. The model behavior during flight was observed by the pitch pilot, located at the side of the test section, and by the yaw and roll pilot, located in the rear of the test section (see fig. 3). The results obtained in the flight tests were primarily in the form of qualitative ratings of the flight behavior based on pilots' opinions. Motion-picture records were obtained in the tests for subsequent study and to verify and correlate the ratings for the different flight conditions. The model was flown over an angle-of-attack range from 6° to 28°. For most of the flights the center of gravity was located at $0.28\bar{c}$. A few flights were made to determine the effect of the center-of-gravity location at an angle of attack of 12°. The control deflections used in most of the flight tests were $\pm 10^{\circ}$ for elevator, $\pm 15^{\circ}$ for rudder, and $\pm 15^{\circ}$ on each elevon for roll control. In some flights a roll damper, having a rate gyro as the sensing element, was used to provide artificial damping in roll.

Force Tests

Static and dynamic force tests were made to determine the static stability and control characteristics and the dynamic stability derivatives of the model for correlation with the flight-test results. The static and dynamic force tests generally were made over an angle-of-attack range from -4° to 40°. The static lateral stability characteristics were determined both from the incremental differences in C_n, C_l, and C_Y measured over the angle-of-attack range at fixed angles of sideslip of $\pm 5^{\circ}$ and from measurements over a sideslip-angle range at fixed angles of attack. The dynamic longitudinal stability derivatives were measured for a pitch amplitude of ± 0.069 radian and for frequencies of 0.35 and 0.70 cps corresponding to values of the reduced-frequency parameter k of 0.103 and 0.206, respectively. The dynamic lateral stability derivatives were measured for an amplitude of ± 0.087 radian in both roll and yaw for frequencies of 0.45, 0.70, and 0.90 cps corresponding to values of k of 0.168, 0.260, and 0.339, respectively.

The force tests were conducted at a dynamic pressure of 2.80 lb/ft^2 (134.6 N/m^2), which corresponds to a Reynolds number of 1.43×10^6 based on the mean aerodynamic chord. The model was so small in proportion to the tunnel test section that no wind-tunnel corrections were needed.

Calculations

Linearized three-degree-of-freedom longitudinal-stability equations of motion as presented in reference 4 were used to calculate the period and damping of the phugoid and short-period oscillations and the damping of the longitudinal aperiodic modes.

Dynamic lateral stability calculations were also made by using the linear three-degree-of-freedom lateral-stability equations as presented in reference 4 to determine the period and damping of the Dutch roll oscillation and the damping of the lateral aperiodic modes. In addition, the roll-angle-to-side-velocity parameter $\left|\phi/v_e\right|$ and the inverse cyclic damping $1/C_{1/2}$ were determined and the results compared with the handling-qualities requirements of reference 5. As part of the lateral study, six-degree-of-freedom nonlinear equations similar to those presented in reference 6 were used to obtain time histories of the lateral motion subsequent to step aileron inputs.

All the stability calculations and motion studies were made with the use of the stability derivatives measured in the force-test part of the investigation.

FORCE-TEST RESULTS AND DISCUSSION

Longitudinal Stability and Control

The basic static longitudinal stability data for the model are presented in figure 5. The data show that the model had static longitudinal stability at low and high angles of attack, but had an unstable break in the pitching-moment curve at moderate angles of attack (from about 20° to 25°). This longitudinal instability was much more pronounced with the leading-edge flaps deflected than with the leading-edge flaps up (undeflected). This type of instability at low speeds is not generally characteristic of delta wings and is apparently associated with some flow interference effect between the forward delta and the rear delta. Figure 5 also shows that deflecting the leading-edge flaps reduced the lift-curve slope at low angles of attack, but the model showed the sharp increase in lift-curve slope at moderate angles of attack which is generally characteristic of delta wings at low speeds.

The elevator effectiveness of the model for various combinations of control surfaces is presented in figure 6. In figures 6(a) and 6(b) data are presented for full-span elevon deflection for the model with the leading-edge flaps up and down, respectively. These data show that the elevon surfaces are a very effective pitch control and provide more than enough moment to trim the model over the test angle-of-attack range. The data presented in figures 6(c) and 6(d) show that each of the trailing-edge surfaces was effective for pitch trim.

The oscillatory stability derivatives measured in the pitching oscillation tests are presented in figure 7. The in-phase derivatives are presented in figure 7(a) and

generally show reasonable agreement with static data (k = 0). The out-of-phase derivatives, presented in figure 7(b), show that the model had positive damping in pitch (negative values of $C_{m_q} + C_{m_{\dot{\alpha}}}$) throughout the test angle-of-attack range and that the damping generally increased with increasing angle of attack.

Lateral Stability and Control

The static lateral stability data are presented in figures 8 and 9. The data of figure 8 show that the variations of C_l, C_n, and C_Y with changes in sideslip angle are generally linear at low sideslip angles ($\beta \approx \pm 5^\circ$) over the test angle-of-attack range. The data presented in figure 9 were determined from the incremental differences in C_l, C_n, and C_Y measured over the angle-of-attack range at fixed sideslip angles of $\pm 5^\circ$ and show that the model had directional stability ($+C_{n_\beta}$) at the lower angles of attack but was directionally unstable ($-C_{n_\beta}$) at angles of attack above about 17°. The model had positive dihedral effect ($-C_{l_\beta}$) up to an angle of attack of about 27°.

Presented in figure 10 are data showing the aileron effectiveness for various combinations of control surfaces. The data show that the rolling moment produced by the ailerons remained about constant over the test angle-of-attack range. Comparing the effects of the outboard surfaces with the inboard surfaces, it can be seen that although the outboard surfaces produced larger rolling moments, the inboard surfaces produced more favorable yawing-moment characteristics. The proverse (favorable) yawing moment produced by the inboard surfaces has been noted in previous investigations with other models and was attributed to the aerodynamic loading induced on the vertical tail by differential elevon deflection (ref. 7).

The rudder effectiveness data for the model are presented in figure 11. These data show that the effectiveness of the rudder remained essentially constant throughout the test angle-of-attack range.

The lateral oscillatory stability derivatives measured in the yawing oscillation tests are presented in figure 12. The in-phase yawing derivatives, presented in figure 12(a), are in good agreement with the static lateral derivatives (k = 0), particularly at the lower angles of attack. The out-of-phase yawing derivatives, presented in figure 12(b), show that the model had positive damping in yaw (negative values of $C_{n_r} - C_{n_{\dot{\beta}}} \cos \alpha$) except at an angle of attack of 30°. Deflecting the leading-edge flaps downward 40° had very little effect on the yawing derivatives.

The lateral oscillatory stability derivatives measured in rolling oscillation tests are presented in figure 13. The in-phase rolling derivatives, presented in figure 13(a), are in good agreement with the static derivatives (k = 0). The out-of-phase derivatives, presented in figure 13(b), show that the model had positive damping in roll (negative

values of $C_{l_p} + C_{l_{\dot{\beta}}} \sin \alpha)$ that remained constant, in effect, throughout the test angle-of-attack range. Deflecting the leading-edge flaps downward 40° had little effect on the rolling derivatives.

FLIGHT-TEST RESULTS AND DISCUSSION

A motion-picture film supplement (L-970) covering the flight tests of the model has been prepared and is available on loan. A request card form and a description of the film are found at the end of this report.

Interpretation of Flight-Test Results

In the flying model technique there are several factors which must be considered in correlating the results of the model to those of a full-scale airplane. The first factor, and probably the most important, is that the angular motions of a dynamic model are much more rapid than those of its full-scale counterpart. These rapid motions give the model pilot less time in which to apply a corrective control. Also, inasmuch as the model pilot is remotely located, he cannot feel the acceleration that a full-scale pilot would experience. The lack of feel of the acceleration introduces considerable lag in the model pilot's application of control since he must, instead, rely on visual observations of some model displacements before he recognizes the need for corrective control. In addition, the fact that the model must be flown within the confines of the tunnel test section prohibits the model pilot from allowing the development of certain mild drifting motions or slight changes in speed which would be of little concern to the pilot of a full-scale airplane. These factors, which combine to make the model more difficult to fly than the full-scale airplane, can be offset somewhat by the use of flicker (full on or off) control to minimize the time lag involved in obtaining corrective response.

In the past it has been found that this flying model technique gave a good qualitative indication of the dynamic behavior of an airplane and of the relative ease of control. The models flown were about 6 feet (1.8 meters) in length and were generally 1/10-scale versions of fighter-type airplanes or moderately sized transport or bomber airplanes. The fact that good correlation between the model and full-scale-airplane flight results was obtained is an indication that the rapid motions of the model were properly offset by the increase in control sensitivity to give a good simulation of the behavior of the airplane. Recently, however, when these models were used to simulate larger airplanes such as the supersonic transport, it was found that the model-flight-test results were somewhat optimistic. For example, in the model flight tests these configurations were generally found to have satisfactory dynamic behavior whereas the simulator studies showed them to have poor flight behavior because of sluggish initial control response (see refs. 8, 9, and 10). Analysis of these results indicates that the apparent discrepancy between the

model and simulator flight data is related to the improper control power simulation in the model. That is, the flicker control used to offset the rapid model motions gave too much control to simulate properly the sluggish control response generally characteristic of very large airplanes with high moments of inertia. Therefore, the model flight results presented herein are somewhat optimistic for the basic airplane configuration, but they should give a fairly good indication of the flight behavior of the airplane configuration wherein control-column-to-elevator gearings have been optimized in order to achieve satisfactory control response.

Longitudinal Stability and Control

The longitudinal stability characteristics of the basic model ($\delta_n = 0^o$) were found to be generally satisfactory in the angle-of-attack range from 6^o to 15^o for the design allowable center-of-gravity range ($0.28\bar{c}$ to $0.31\bar{c}$). The model was dynamically longitudinally stable, was easy to fly, and required little attention to the pitch control. The longitudinal control was adequate for maneuvering or correcting for disturbances at the low angles of attack; however, it became progressively less effective as the angle of attack was increased. The control power of this clean (flaps up) configuration, although relatively weak, was considerably better than that of an arrow-wing supersonic transport configuration reported in reference 8. The reason for the increased control effectiveness of the present model was that the control surfaces of the present model were much larger than those of the arrow-wing model. As the angle of attack was increased above 15^o, there was a noticeable reduction in the longitudinal stability; and, near an angle of attack of 20^o, the model appeared to be about neutrally stable with the center of gravity at $0.28\bar{c}$ and slightly unstable with the center of gravity at $0.31\bar{c}$. Even though at times the flight behavior of the model was somewhat unsteady, the motions seemed to be fairly well damped, and sustained flights could be made by careful attention to the control. At an angle of attack of about 25^o, the model appeared to become more stable and was much steadier and easier to fly. (These flight-test results are generally substantiated by the static stability and control data presented in figs. 5 and 6.) At the higher angles of attack, the control was considered to be very weak and it was necessary to increase the control deflection from $\pm 5^o$ to $\pm 10^o$. Attempts to fly the model above an angle of attack of about 28^o were generally terminated by a divergence in yaw. This divergence in yaw will be discussed subsequently in this report.

The flight characteristics of the model with leading-edge flaps down ($\delta_n = -40^o$) were generally similar to those of the basic model ($\delta_n = 0^o$), although at low and moderate angles of attack deflecting the leading-edge flaps improved the static longitudinal stability and made the model easier to fly. An increase in angle of attack, however, caused the model to become unsteady longitudinally and careful attention to the controls was required because of static longitudinal instability. The instability at angles of attack from about

20° to 25° was greater than that for the clean configuration even though no strong pitch-up tendency was experienced, and sustained flights were possible with careful attention to the controls. As in the clean configuration, an increase in angle of attack above about 25° provided an improvement in flight behavior because of an increase in static longitudinal stability and damping in pitch (see figs. 5, 6, and 7). Flights above an angle of attack of about 28° were terminated by a divergence in yaw.

As part of the flight investigation, tests were made to determine the effect of static margin on the longitudinal flight characteristics of the basic model ($\delta_n = 0^{\circ}$). These tests were made at an angle of attack of 12°. The results of the tests showed that the model had good longitudinal stability characteristics and adequate control with the center of gravity in the range from $0.24\bar{c}$ to $0.28\bar{c}$ (static margin between 8 and 4 percent $\bar{c}$). When the center of gravity was moved rearward to $0.31\bar{c}$ (static margin of 1 percent $\bar{c}$), the model, as expected, was a little less steady longitudinally and was somewhat more sensitive to control; therefore, it required more attention to fly smoothly. There was a marked deterioration in the longitudinal stability and control characteristics as the center of gravity was moved rearward to $0.37\bar{c}$ (negative static margin of 5 percent $\bar{c}$). Sustained flights were possible with this amount of negative static margin, but the model motions were somewhat erratic and the pilot had to use extreme care to keep the amplitudes of the motions small by constant attention to the controls. With the center of gravity moved back to $0.39\bar{c}$ (negative static margin of 7 percent $\bar{c}$), the model was flyable but only if the disturbances were small. Any large control input or gust which caused the model to pitch appreciably away from its trimmed attitude generally led to loss of control, and the model diverged in pitch because the control was not powerful enough to overcome the static longitudinal instability. Flights were attempted with the center of gravity moved back to $0.41\bar{c}$ (negative static margin of 9 percent $\bar{c}$) but were found to be impossible.

Presented in figure 14 are calculated values of the period and the reciprocal of the time to damp to half-amplitude of the longitudinal modes of motion of the full-scale configuration. In the low-angle-of-attack range, the configuration has the characteristic short-period oscillation and the long-period or phugoid oscillation. As the angle of attack was increased, however, both of these oscillations broke down into two aperiodic modes and one mode from the short-period oscillation combined with another mode from the phugoid oscillation to form a third oscillation. This third oscillation, which is discussed in references 4, 11, and 12, has the period of the phugoid oscillation and the damping of the short-period oscillation. It is interesting to note that one of the aperiodic modes from the phugoid oscillation became unstable near an angle of attack of 16° and reached a maximum value of negative damping near an angle of attack of 20°. It should also be noted that for the flaps-deflected configuration ($\delta_n = -40^{\circ}$) this unstable

aperiodic mode shows a time to double amplitude of about 1 second (model scale); however, there was no real problem in flying the model through this unstable region.

The results of calculations to show the effect of the center-of-gravity location on the longitudinal modes of motion for the basic model $(\delta_n = 0^o)$ are given in figure 15. This information is presented at an angle of attack of 12^o from both two-degree-of-freedom and three-degree-of-freedom calculations. In the past, the two-degree-of-freedom analysis has been used almost exclusively to establish the relationship between the short-period mode of motion and the stick-fixed maneuver point for rearward center-of-gravity conditions. The results of figure 15 (as well as those of refs. 4, 11, and 12) show, however, that the two-degree-of-freedom case is not valid for analysis purposes because of the interaction of the short-period and phugoid modes under negative static margin conditions. The one mode that does appear to be significant in limiting the rearward center-of-gravity movement under this condition is the unstable aperiodic mode which is shown in the three-degree-of-freedom analysis case. The instability of this mode appears to increase in almost direct proportion to the increase in negative static margin. It is interesting to note that at the rearward center-of-gravity position at which flight tests became impossible, this mode shows a time to double amplitude of about 0.5 second (model scale) for the three-degree-of-freedom analysis and about 0.7 second for the two-degree-of-freedom analysis.

Lateral Stability and Control

In brief, the flight tests showed that the model was directionally stable and that the Dutch roll oscillation was generally well damped throughout most of the test angle-of-attack range. At high angles of attack, however, the Dutch roll oscillation became lightly damped and the directional stability deteriorated and flights were generally terminated near an angle of attack of 28^o by a divergence in yaw. The tests also showed that the full-span trailing-edge control surfaces on the model provided adequate roll control, but the effectiveness of these surfaces deteriorated with increasing angle of attack and the control was relatively weak at the highest angle of attack flown.

Specifically, in the angle-of-attack range from 6^o to 20^o the Dutch roll oscillation was well damped. As the angle of attack increased, there was a progressive deterioration in the Dutch roll damping and near an angle of attack of 25^o the Dutch roll oscillation became lightly damped. Near an angle of attack of 28^o the Dutch roll oscillation appeared to be neutrally damped and at times the model flew with a small constant amplitude rolling oscillation. Deflecting the leading-edge flaps downward produced a noticeable reduction in lateral damping at moderate angles of attack but the variation of the Dutch roll characteristics with angle of attack for this condition was generally similar to that for the basic model.

The use of a roll-rate damper to provide artificial stabilization in roll gave a marked improvement in the flight characteristics of the model at the higher angles of attack where the inherent damping of the basic model was low. At the lower angles of attack the effect of the roll-rate damper on the flight characteristics was not as noticeable as that for the higher angles of attack but the model was easier to fly with the increased damping because it was less sensitive to the gustiness of the tunnel.

Presented in figure 16 are calculated period and damping characteristics of the Dutch roll oscillation for the full-scale configuration. These results show that the Dutch roll oscillation was stable over most of the test angle-of-attack range. The data for the basic model show almost constant damping with increasing angle of attack up to about 20° and then a rapid deterioration in damping at the higher angles of attack. These results indicate fairly good Dutch roll damping over most of the angle-of-attack range and are generally in good agreement with the flight-test results.

In order to show a comparison of the calculated Dutch roll damping of this configuration with military specifications for flying qualities of piloted airplanes (see ref. 5), the calculated data of figure 16 have been plotted in figure 17 in terms of the inverse cyclic damping $\left(1/C_{1/2}\right)$ and the roll-angle-to-side-velocity ratio $\left|\phi/v_e\right|$. The upper boundary of this plot specifies the value of $1/C_{1/2}$ required for satisfactory Dutch roll damping. The lower boundary specifies the minimum damping acceptable when augmentation devices required for satisfactory damping are inoperative. The results of this figure show that the Dutch roll damping of the configuration was satisfactory at the lower angles of attack but, at the higher angles of attack, the damping was generally unacceptable for normal operation.

The directional stability characteristics of the model were generally very good at low and moderate angles of attack but at angles of attack of about 25° the directional stability was noted to deteriorate rapidly and near an angle of attack of 28° flights were generally terminated by a divergence in yaw against full corrective control. A comparison of the static lateral data of figure 9 with the flight-test data showed that the angle of attack for zero static directional stability (17°) was much lower than that at which the model actually diverged in flight (28°). This result has been noted in other investigations in which configurations having high positive effective dihedral in combination with large ratios of I_Z/I_X were flown. In such cases, the dynamic directional stability parameter $\left(C_{n_{\beta,\text{dynamic}}}\right)$ was generally found to provide a much better correlation with the model-flight-test directional stability characteristics.

Values of $C_{n_{\beta,\text{dynamic}}}$ for the present model have been calculated and are presented in figure 18. These results show that the angle of attack for $C_{n_{\beta,\text{dynamic}}} = 0$ was about 27° for the basic configuration and about 29° for the configuration with

leading-edge flaps deflected. These results are in good agreement with the model-flight-test results.

The lateral control characteristics of the model were generally satisfactory over the test angle-of-attack range when the full-span elevon surfaces were used for control. In the low-angle-of-attack range, the lateral control was very effective for overcoming disturbances and for maneuvering the model within the limited area of the tunnel airstream. Smooth flights could be made about as well with ailerons alone as with simultaneous use of the ailerons and rudder, apparently because of the relatively large proverse yaw of the ailerons (see fig. 10). An increase in angle of attack produced a progressive deterioration in the effectiveness of the controls, and it was necessary to increase the control travels of the ailerons from $\pm 15^{\circ}$ to $\pm 20^{\circ}$ and the rudder from $\pm 15^{\circ}$ to $\pm 30^{\circ}$ to provide satisfactory control at the highest angles of attack flown. Flights could be made with the ailerons alone up to an angle of attack near 25° but in the high-angle-of-attack range the control became too weak for maneuvering the model and for recovering from large disturbances. The deterioration in roll control effectiveness at the high angles of attack is attributed, in part, to the decrease in the rolling moment produced by elevon deflection and also to the fact that an adverse sideslip angle is introduced by rolling because the model tends to roll about its X-axis. (This adverse sideslip angle introduces large rolling moments which opposed the control moment through the effective dihedral parameter $-C_{l_\beta}$.) The sideslip generated by this type of rolling motion can become excessive at high angles of attack as indicated in the expression $\sin \beta = \sin \alpha \sin \phi$.

In addition to the flight tests of the model with the full-span ailerons, a few tests were also made to evaluate the effectiveness of various control combinations. From these flights it was generally found that the aileron control was greatly reduced when the inboard surface e_1 was disconnected from the system. This result is apparently related to the fact that the inboard surface produced large proverse yawing moments which were beneficial in flying the model. (See fig. 10.)

The rudder control on the model was found to be effective over the test angle-of-attack range, even up to the high angles of attack where directional instability made flying difficult. This result is in agreement with the static data of figure 11, which shows that the rudder effectiveness remained essentially constant with angle of attack. It was also found that because of the high dihedral effect the rudder was very effective for producing roll angle at the higher angles of attack, and flights could be made with rudder alone with very little pilot effort.

Presented in figure 19 are calculated roll response data for the full-scale configuration using various aileron control combinations. The data were obtained at an angle of attack of 12° and show that the full-span ailerons (e_1, e_2, and e_3) were capable of producing a roll angle of about 17° in 1 second. When just the two outboard surfaces were

used (e_2 and e_3), the roll response was reduced to about 7° in 1 second. It is interesting to note that, with the full-span control or with only the two outboard surfaces (e_1 and e_2), the sideslip angle induced by rolling was adverse (that is, positive values of β in a right roll) although the yawing was proverse. As previously pointed out, this positive sideslip comes about because the vehicle tends to roll about its X-axis and in this type of rolling motion a sideslip is generated which increases with angle of roll and angle of attack.

CONCLUSIONS

From the force- and flight-test investigation to determine the low-speed stability and control characteristics of a 1/20-scale model of a supersonic transport with a double-delta wing, the following conclusions were drawn:

1. The dynamic longitudinal stability and control characteristics of the model were generally satisfactory over the test angle-of-attack range except from about 20° to 25° where neutral or negative static longitudinal stability made flying somewhat difficult.

2. The Dutch roll oscillation was generally well damped throughout most of the test angle-of-attack range but the damping decreased rapidly at angles of attack above about 20°. The use of a roll-rate damper to provide artificial stabilization in roll generally gave satisfactory Dutch roll characteristics over the test angle-of-attack range.

3. The directional stability characteristics were satisfactory over most of the test angle-of-attack range but deteriorated in the high-angle-of-attack range, and flights were generally terminated near an angle of attack of 28° by a divergence in yaw against full corrective control.

4. The lateral control characteristics of the model were satisfactory over the test angle-of-attack range.

5. Although deflecting the leading-edge flaps downward 40° improved the longitudinal stability characteristics slightly and deteriorated the Dutch roll characteristics at some angles of attack, the overall flight characteristics of this configuration were generally similar to those of the basic configuration (flaps undeflected).

Langley Research Center,
National Aeronautics and Space Administration,
Langley Station, Hampton, Va., August 23, 1967,
720-01-00-08-23.

REFERENCES

1. Mechtly, E. A.: The International System of Units – Physical Constants and Conversion Factors. NASA SP-7012, 1964.

2. Chambers, Joseph R.; and Grafton, Sue B.: Static and Dynamic Longitudinal Stability Derivatives of a Powered 1/9-Scale Model of a Tilt-Wing V/STOL Transport. NASA TN D-3591, 1966.

3. Hewes, Donald E.: Low-Subsonic Measurements of the Static and Oscillatory Lateral Stability Derivatives of a Sweptback-Wing Airplane Configuration at Angles of Attack From -10^{o} to 90^{o}. NASA MEMO 5-20-59L, 1959.

4. Etkin, Bernard: Dynamics of Flight. John Wiley & Sons, Inc., 1962.

5. Anon.: Flying Qualities of Piloted Airplanes. Military Specification MIL-F-8785(ASG), Sept. 1, 1954; Amendment-4, Apr. 17, 1959.

6. Grantham, William D.; and Grafton, Sue B.: Effects of Aircraft Relative Density on Spin and Recovery Characteristics of Some Current Configurations. NASA TN D-2243, 1965.

7. Campbell, John P.: The Use of the Horizontal Tail for Roll Control. NACA RM L55L16a, 1956.

8. Freeman, Delma C., Jr.: Low Subsonic Flight and Force Investigation of a Supersonic Transport Model With a Highly Swept Arrow Wing. NASA TN D-3887, 1967.

9. Staff of the Langley Research Center: Determination of Flight Characteristics of Supersonic Transports During the Landing Approach With a Large Jet Transport In-Flight Simulator. NASA TN D-3971, 1967.

10. Grantham, William D.; and Deal, Perry L.: A Piloted Fixed-Base Simulator Study of Low-Speed Flight Characteristics of an Arrow-Wing Supersonic Transport Design. NASA TN D-4277, 1968.

11. Etkin, Bernard: On a Third Mode of Longitudinal Control-Fixed Oscillation. J. Aeron. Sci. (Readers' Forum), vol. 24, no. 1, Jan. 1957, pp. 71-73.

12. Saunders, T. B.: Handling Qualities of Aircraft With Marginal Longitudinal Stability. C.P. No. 837, Brit. A.R.C., 1966.

TABLE I.- MASS AND DIMENSIONAL CHARACTERISTICS OF MODEL

Weight	56.89 lb (253.1 N)
Wing loading	2.68 lb/ft^2 (128.3 N/m^2)
Moment of inertia about the X-axis	1.59 slug-ft^2 (2.16 kg-m^2)
Moment of inertia about the Y-axis	12.68 slug-ft^2 (17.19 kg-m^2)
Moment of inertia about the Z-axis	14.28 slug-ft^2 (19.36 kg-m^2)
Relative-density factor $\left(\mu = \frac{m}{\rho S b}\right)$	6.04
Wing:	
Area reference (basic delta)	21.21 ft^2 (1.97 m^2)
Mean aerodynamic chord	4.60 ft (1.40 m)
Span	5.80 ft (1.77 m)
Area (total)	23.56 ft^2 (2.19 m^2)
Aspect ratio (total delta)	1.43
Aspect ratio (basic delta)	1.59
Taper ratio (basic delta)	0.064
Sweep angle, leading edge (basic delta)	65^o
Sweep angle, trailing edge	-4.37^o
Sweep angle, forward delta	83^o
Root chord	6.89 ft (2.10 m)
Tip chord	0.44 ft (0.134 m)
Vertical tail:	
Span	12.10 in. (0.31 m)
Area	1.56 ft^2 (0.14 m^2)
Mean aerodynamic chord	21.25 in. (0.54 m)
Aspect ratio	0.65
Taper ratio	0.212
Sweep angle, leading edge	60^o
Sweep angle, trailing edge	-15^o
Root chord	30.73 in. (0.78 m)
Tip chord	6.53 in. (0.17 m)

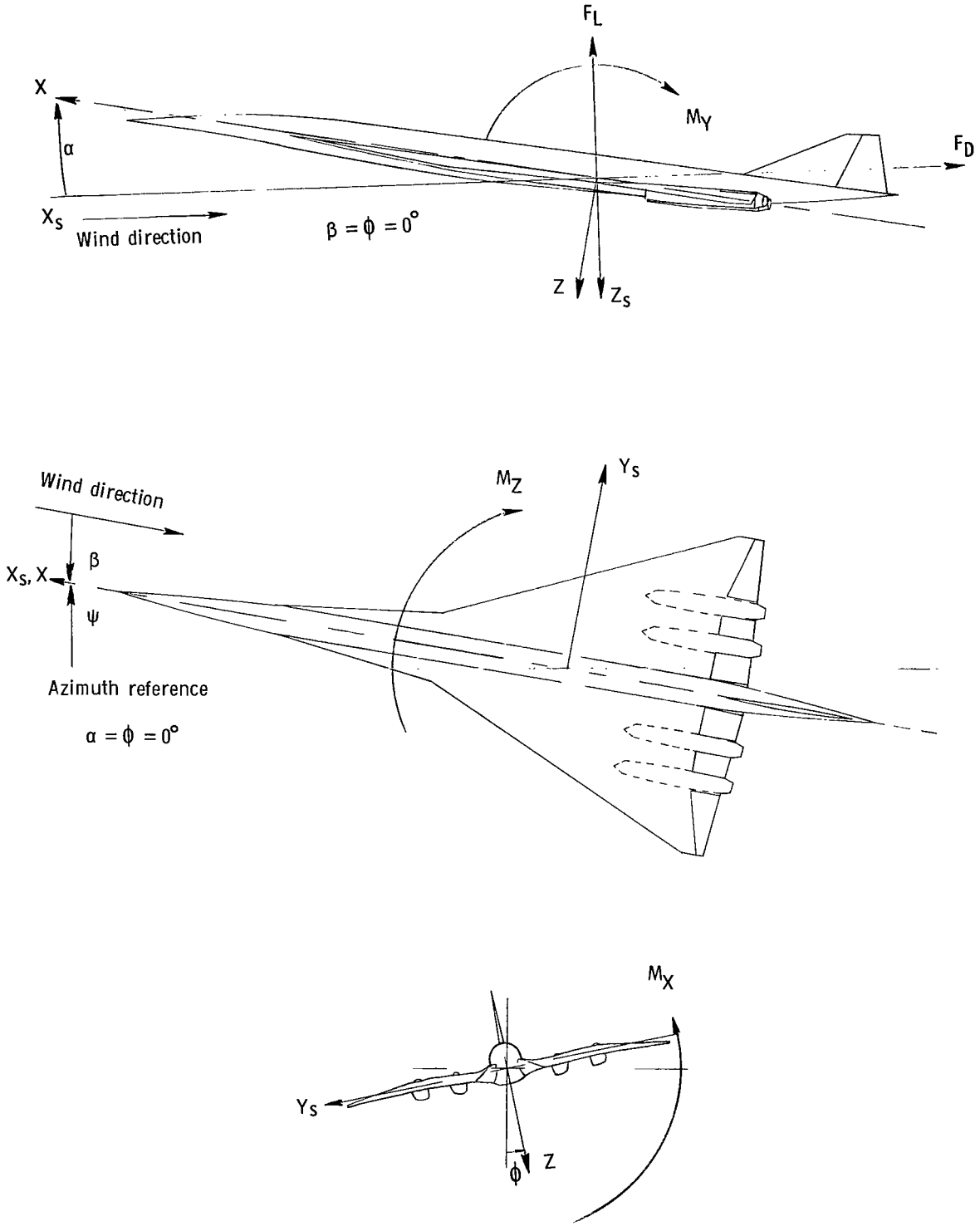

Figure 1.- System of axes used in investigation. Arrows indicate positive directions of moments, forces, and angles.

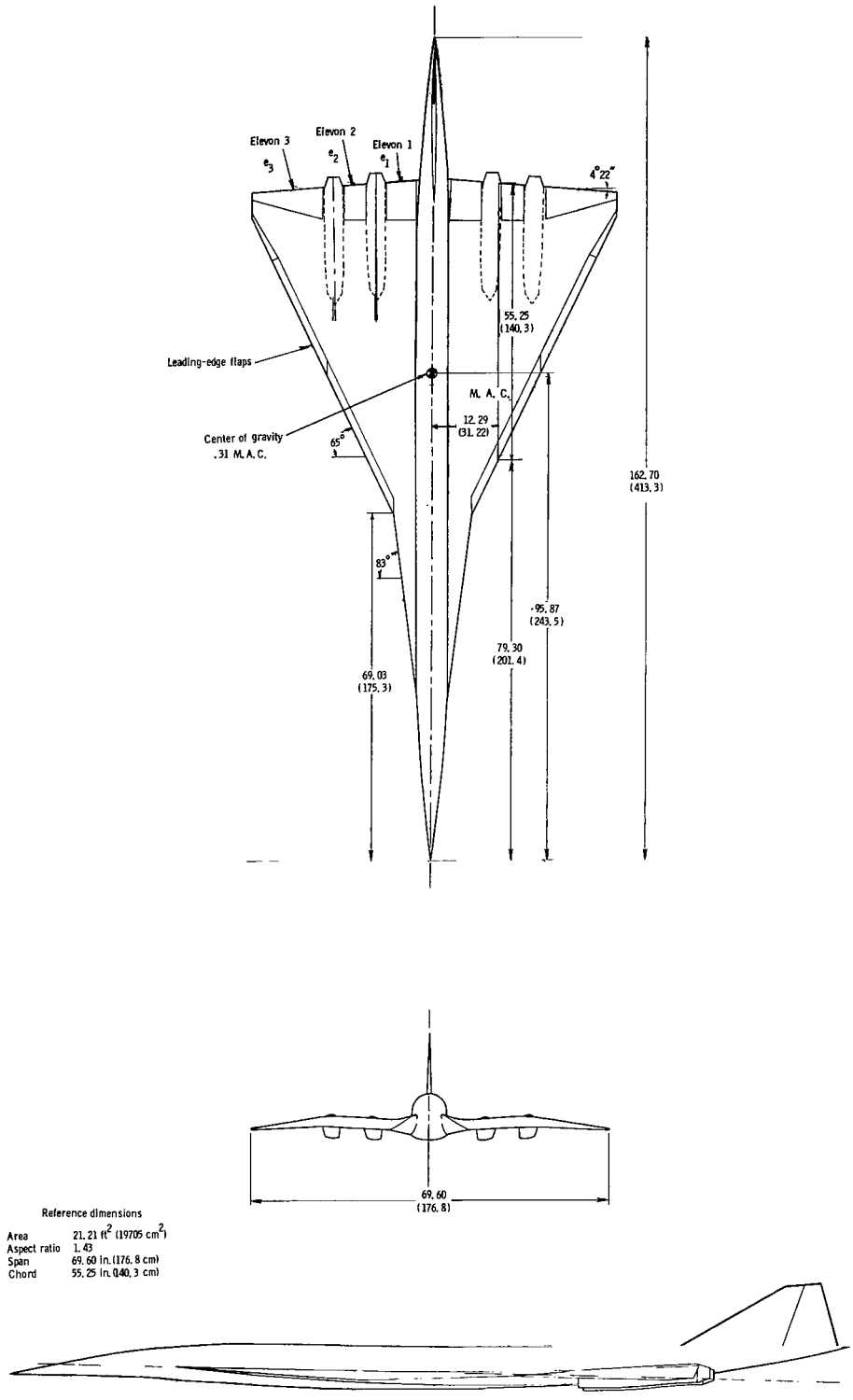

Figure 2.- Three-view drawing of model used in investigation. All dimensions are in inches with centimeters given in parentheses.

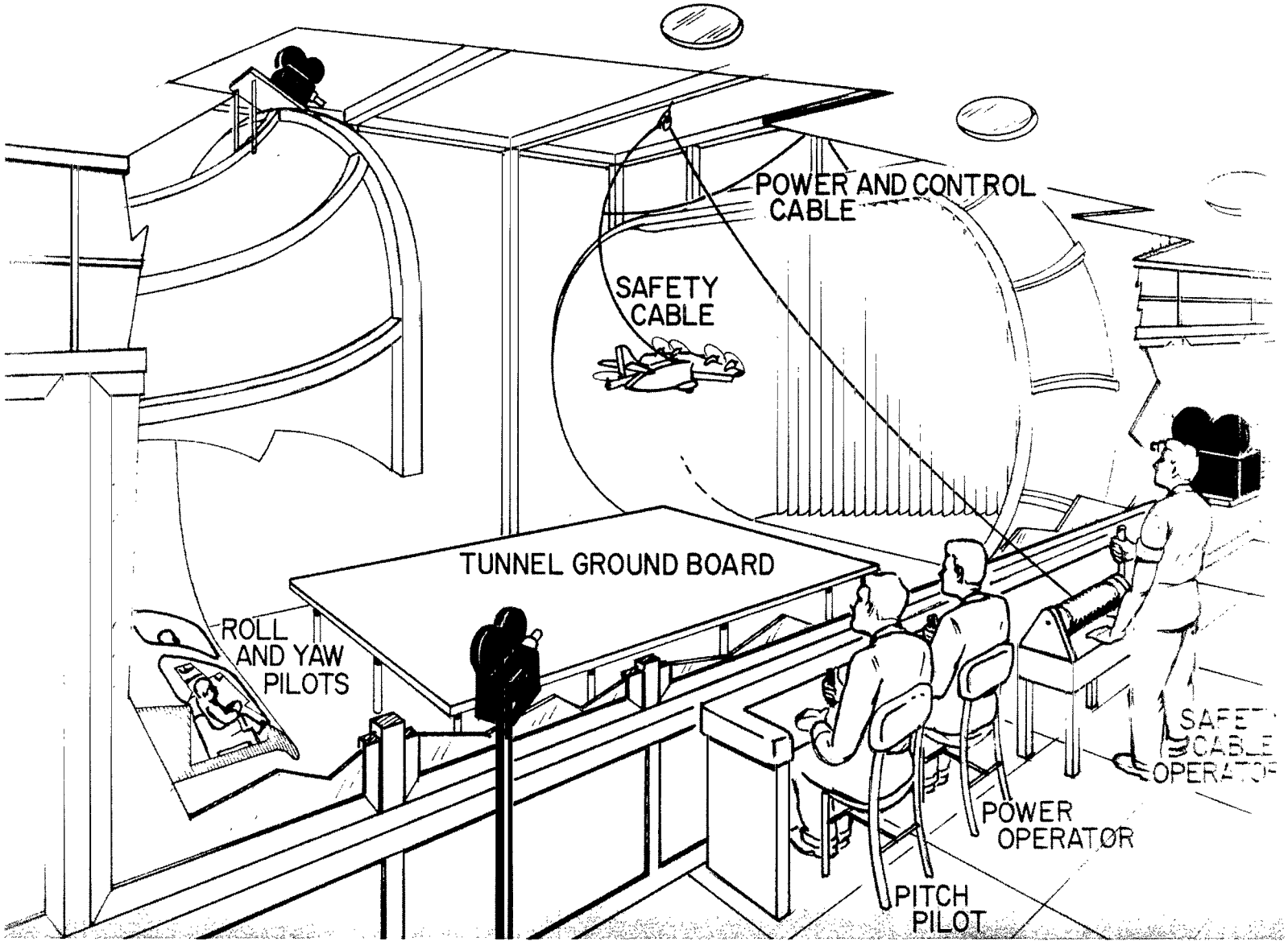

Figure 3.- Test setup for flight tests in the Langley full-scale tunnel. L-64-3008

(a) Model flying in the Langley full-scale tunnel. L-66-4046

Figure 4.- Photographs of the model.

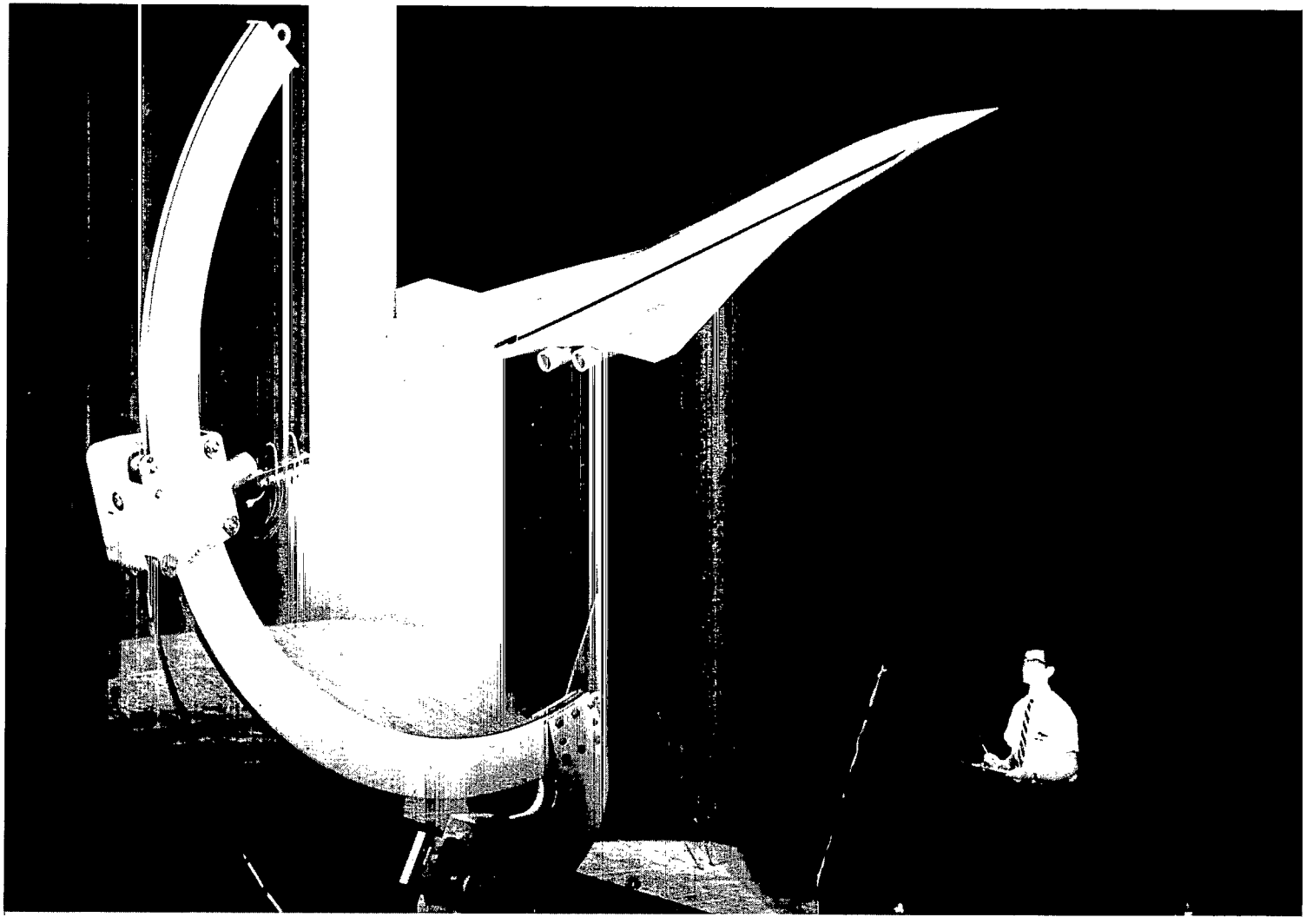

(b) Model mounted on static-force-test equipment in the Langley full-scale tunnel. L-66-8835

Figure 4.- Concluded.

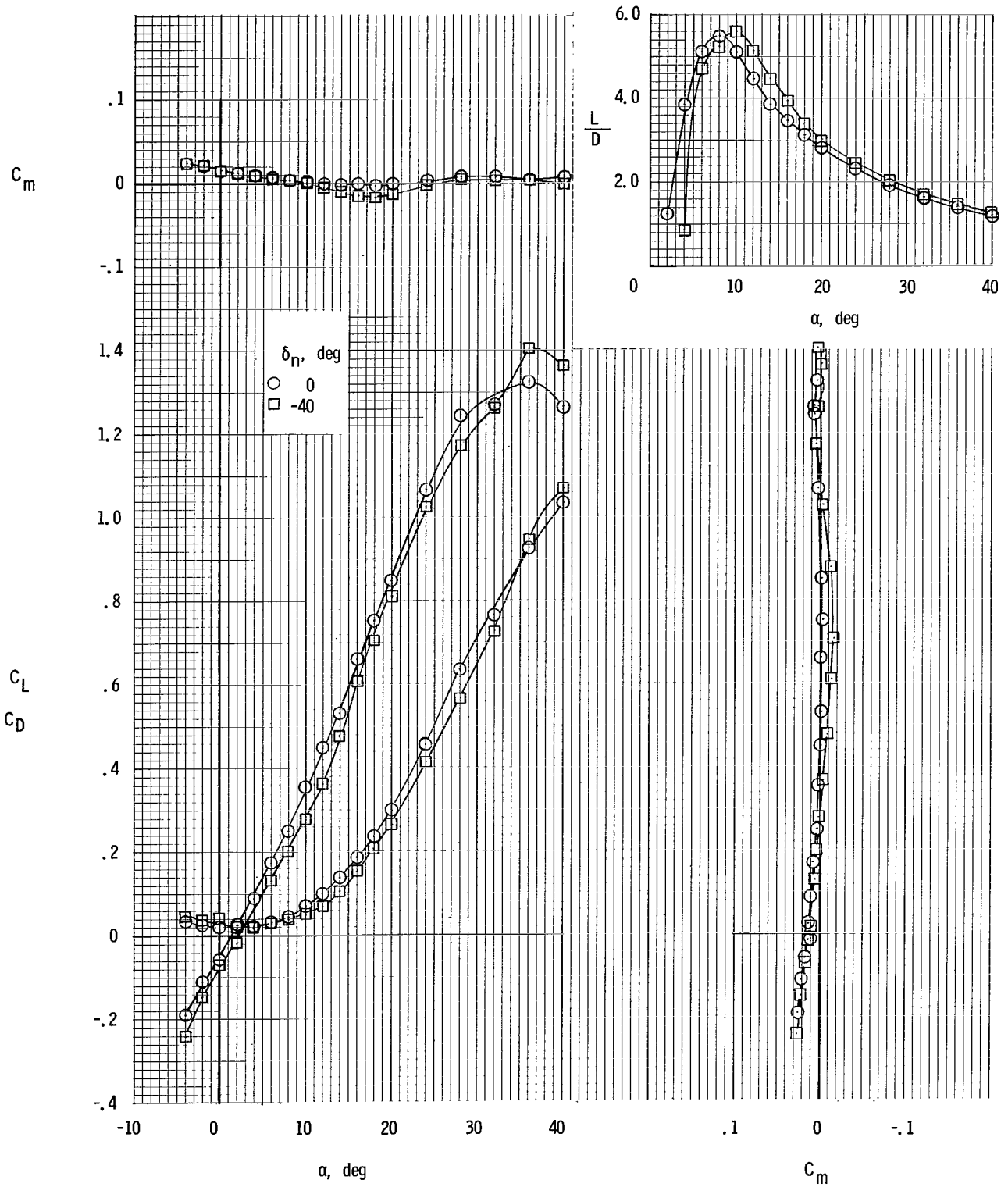

Figure 5.- Static longitudinal stability characteristics of the model.

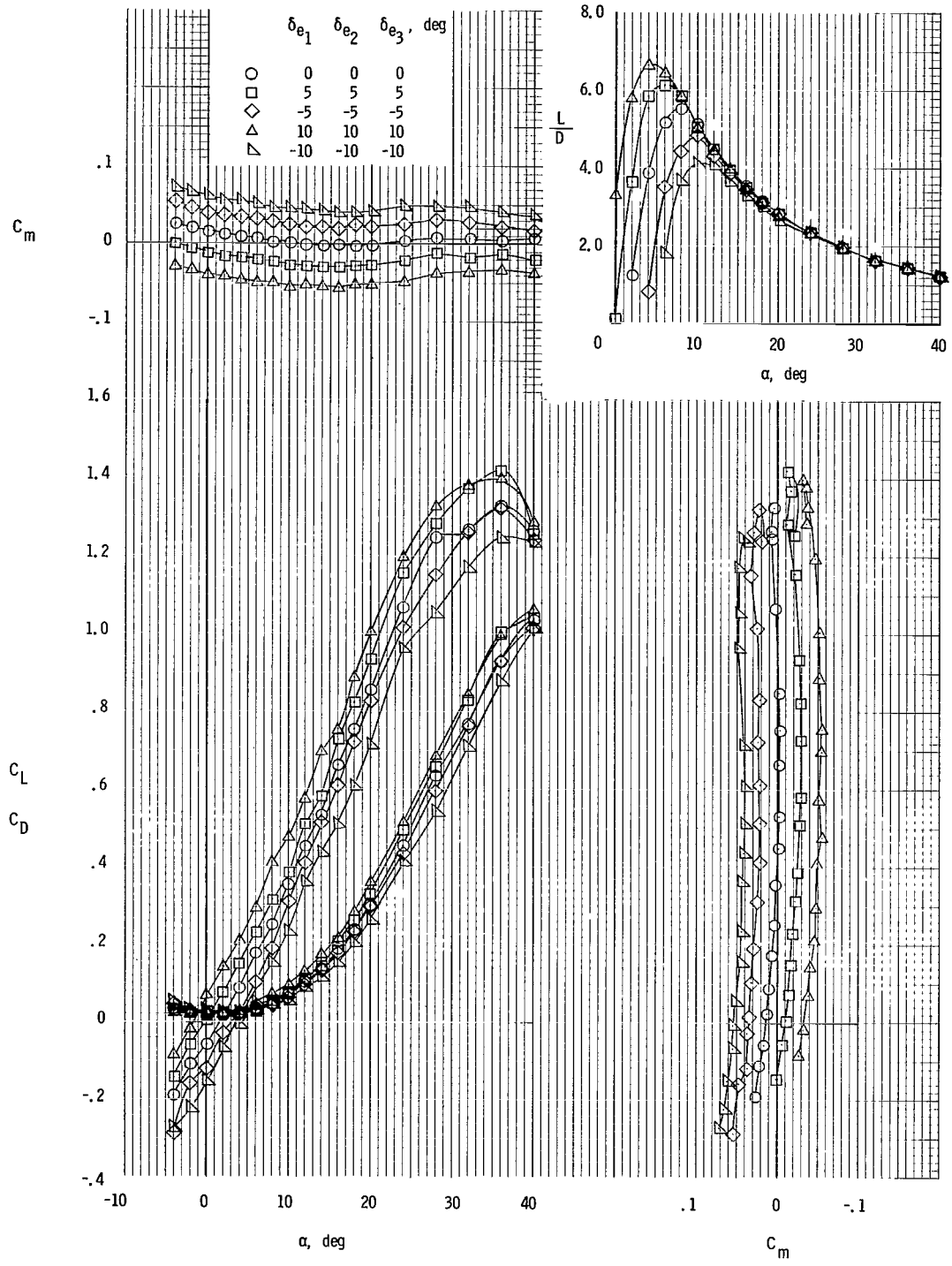

(a) Surfaces e_1, e_2, and e_3. $\delta_n = 0^0$.

Figure 6.- Longitudinal control characteristics of model.

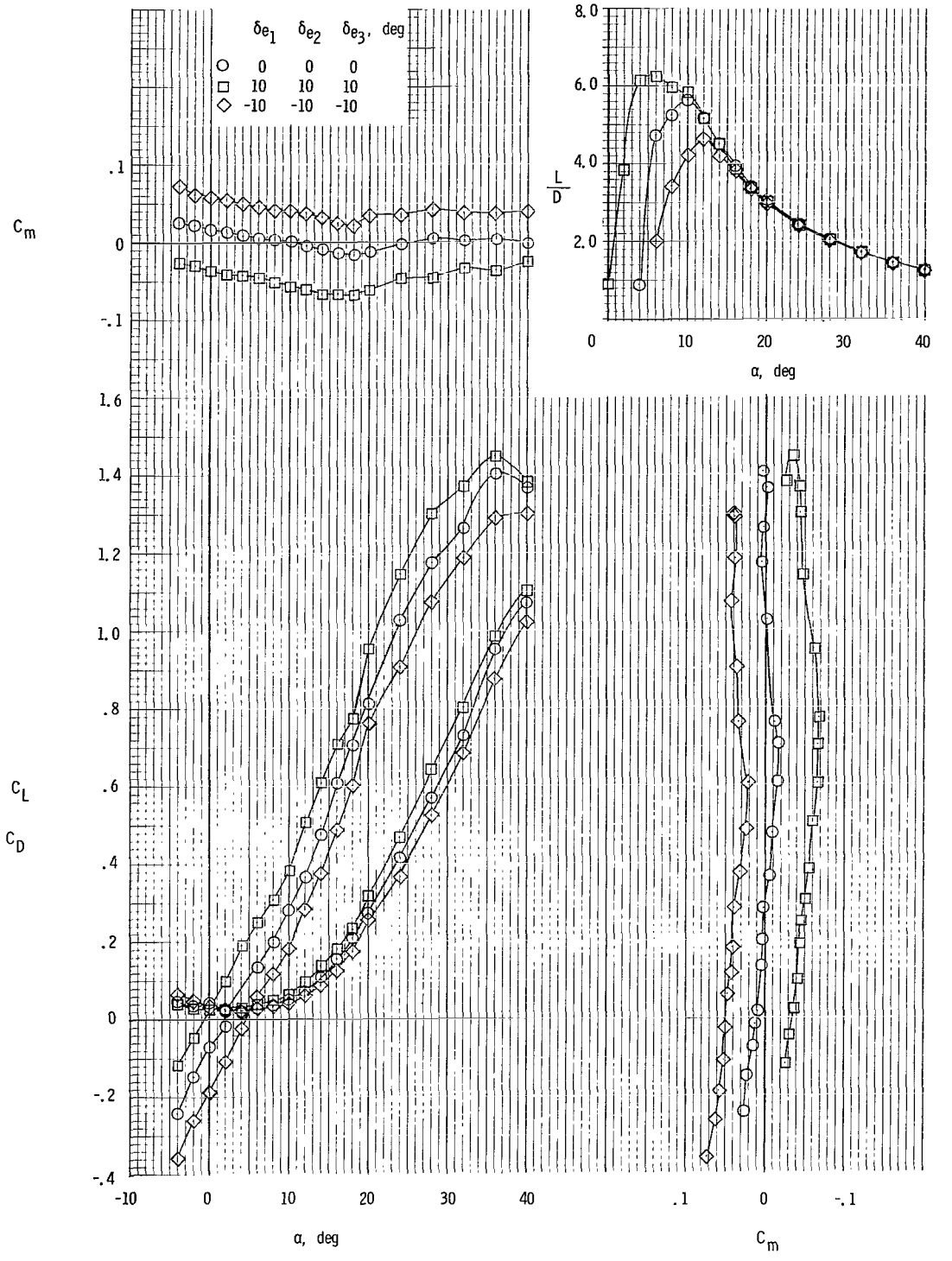

(b) Surfaces e_1, e_2, and e_3. $\delta_n = -40^0$.

Figure 6.- Continued.

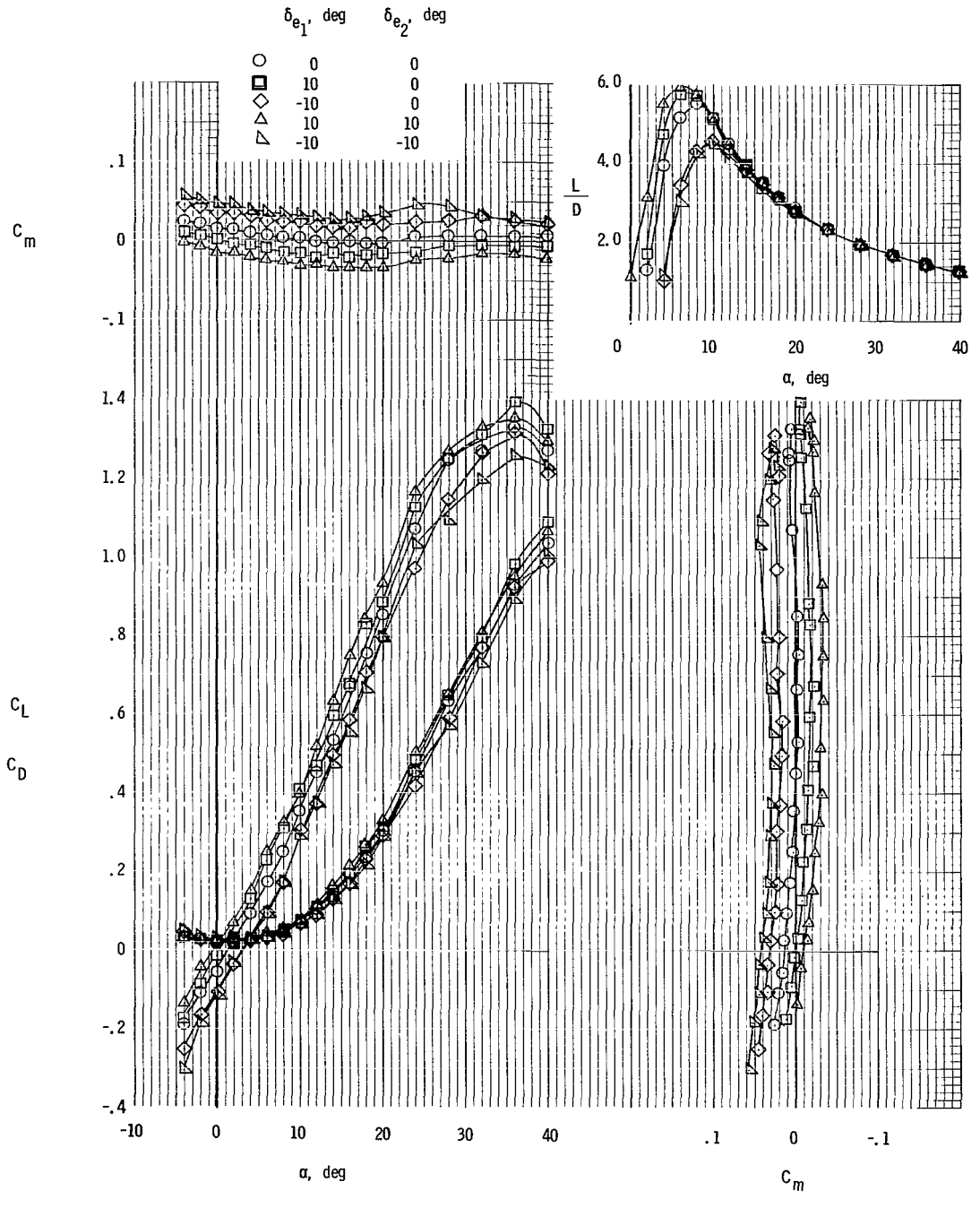

(c) Surfaces e_1 and e_2. $\delta_n = 0^0$.

Figure 6.- Continued.

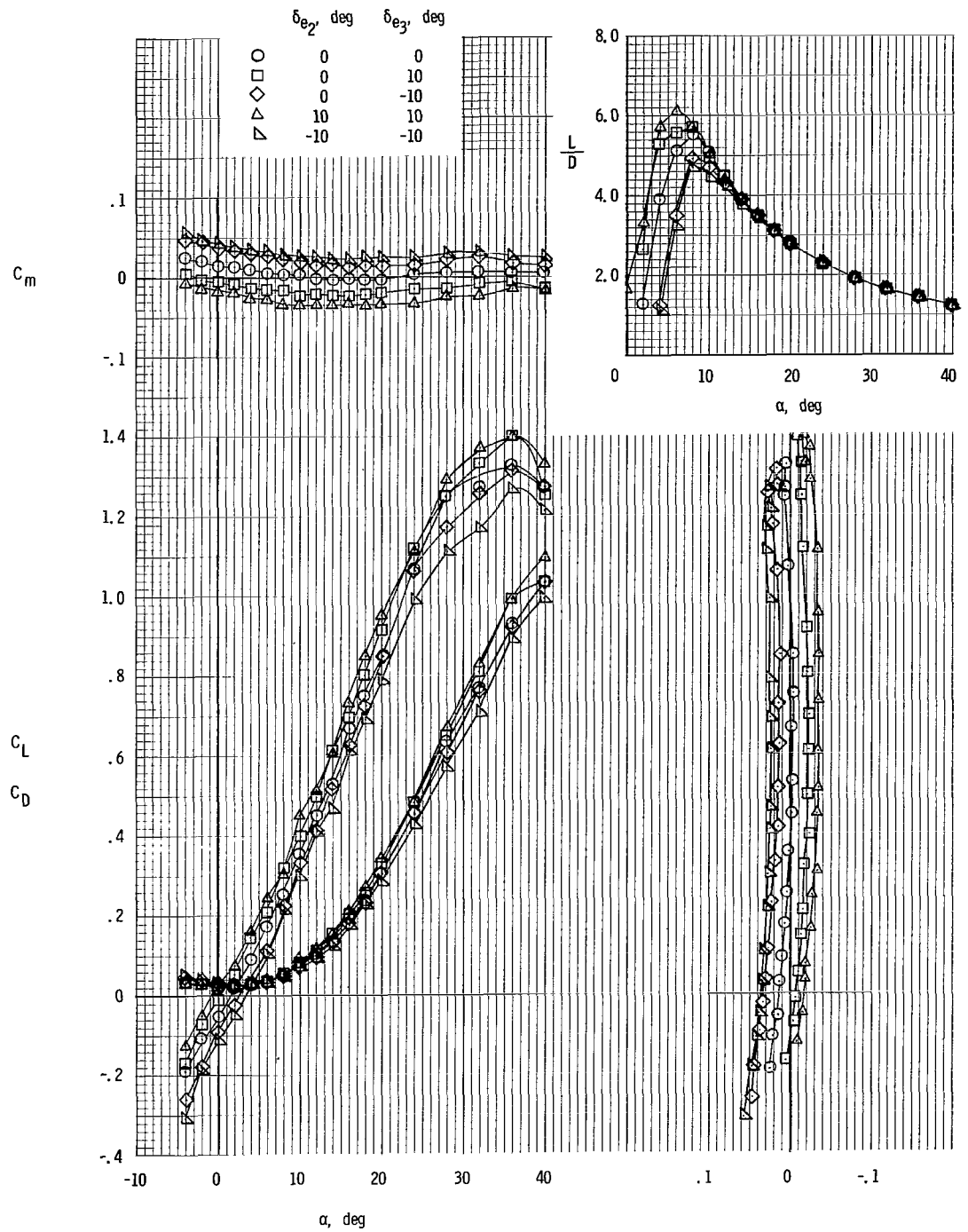

(d) Surfaces e_2 and e_3. $\delta_n = 0^0$.

Figure 6.- Concluded.

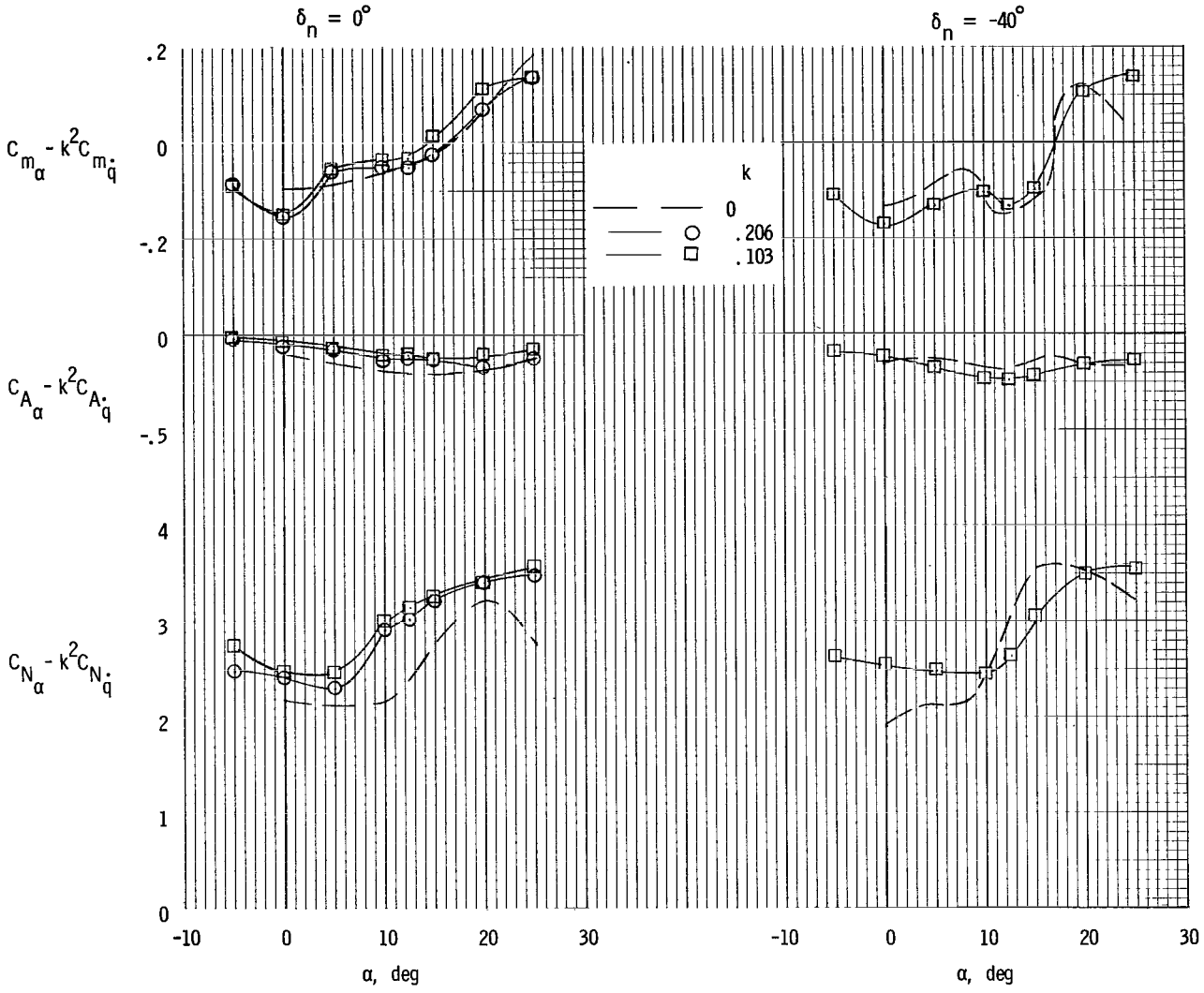

(a) In phase.

Figure 7.- Derivatives measured in pitching oscillation tests.

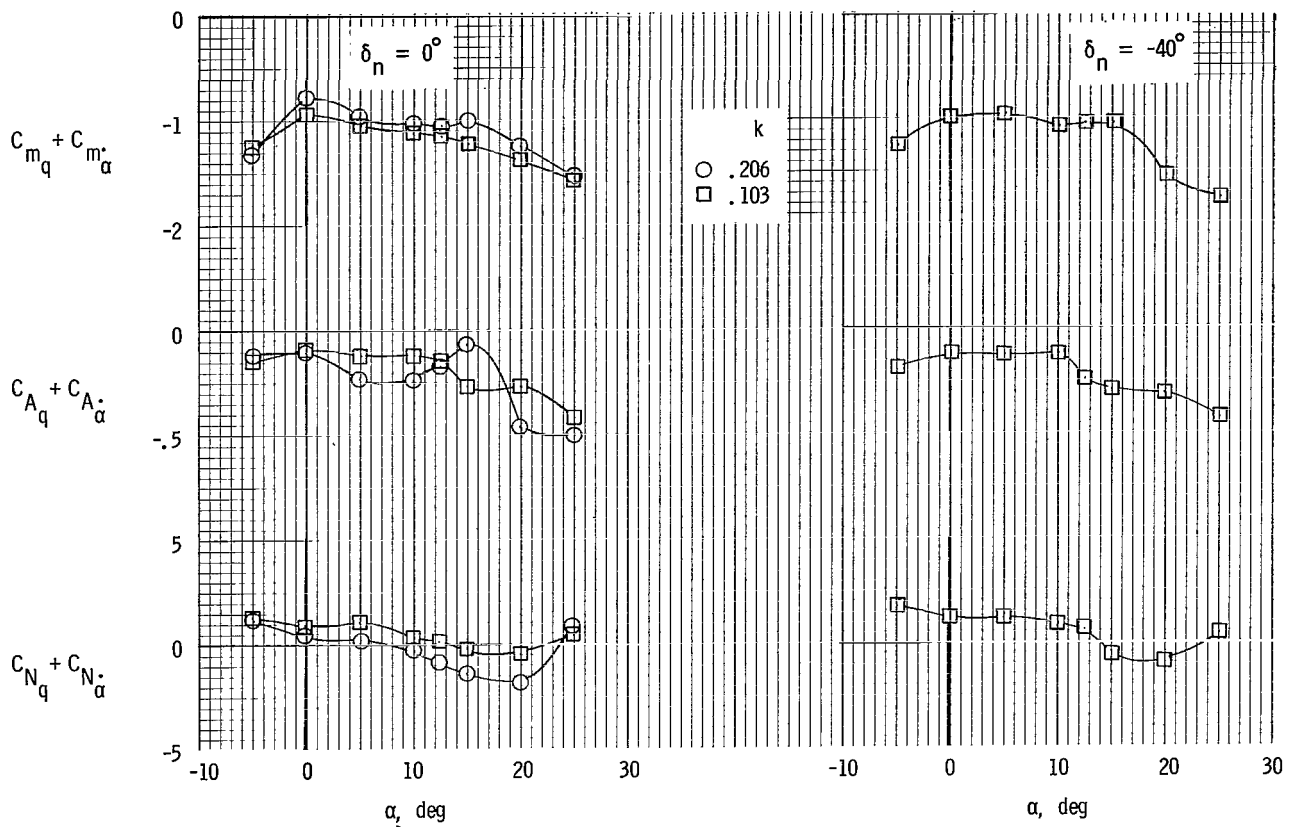

(b) Out of phase.

Figure 7.- Concluded.

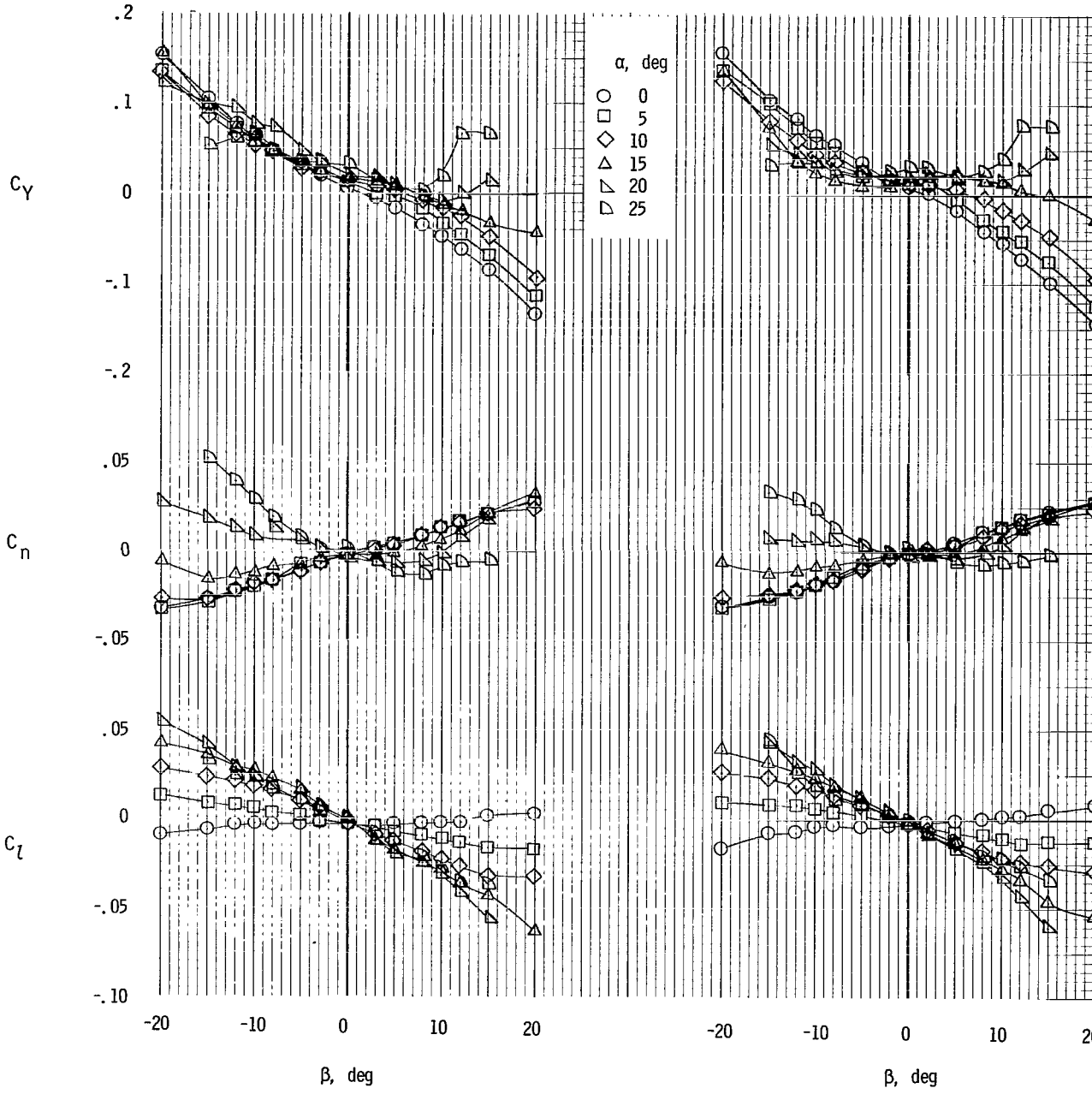

(a) $\delta_n = 0^o$.

(b) $\delta_n = -40^o$.

Figure 8.- Static lateral stability characteristics of the model.

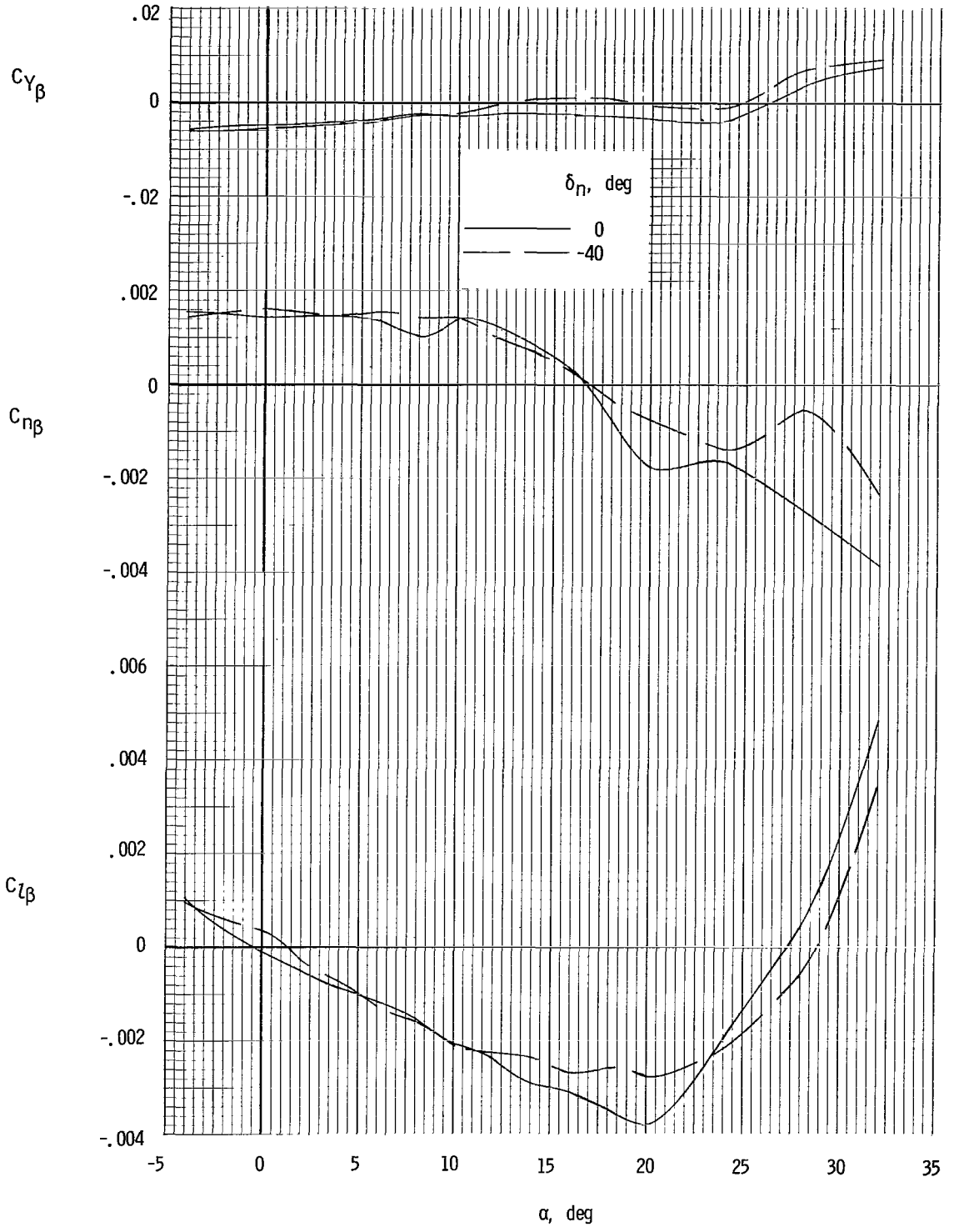

Figure 9.- Static lateral stability derivatives of the model.

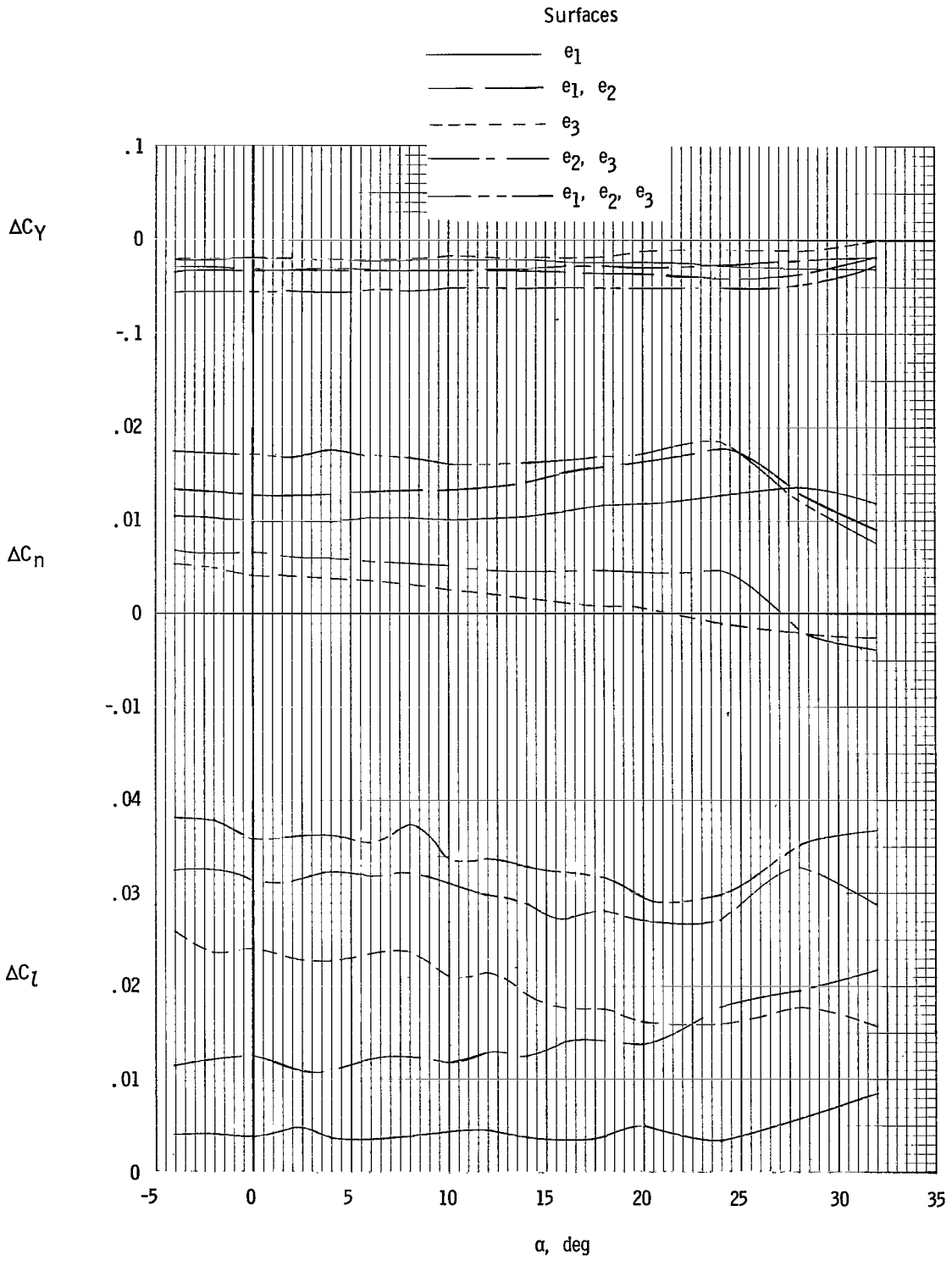

(a) $\delta_n = 0^0$; $\delta_a = 40^0$.

Figure 10.- Total aileron control effectiveness of the model.

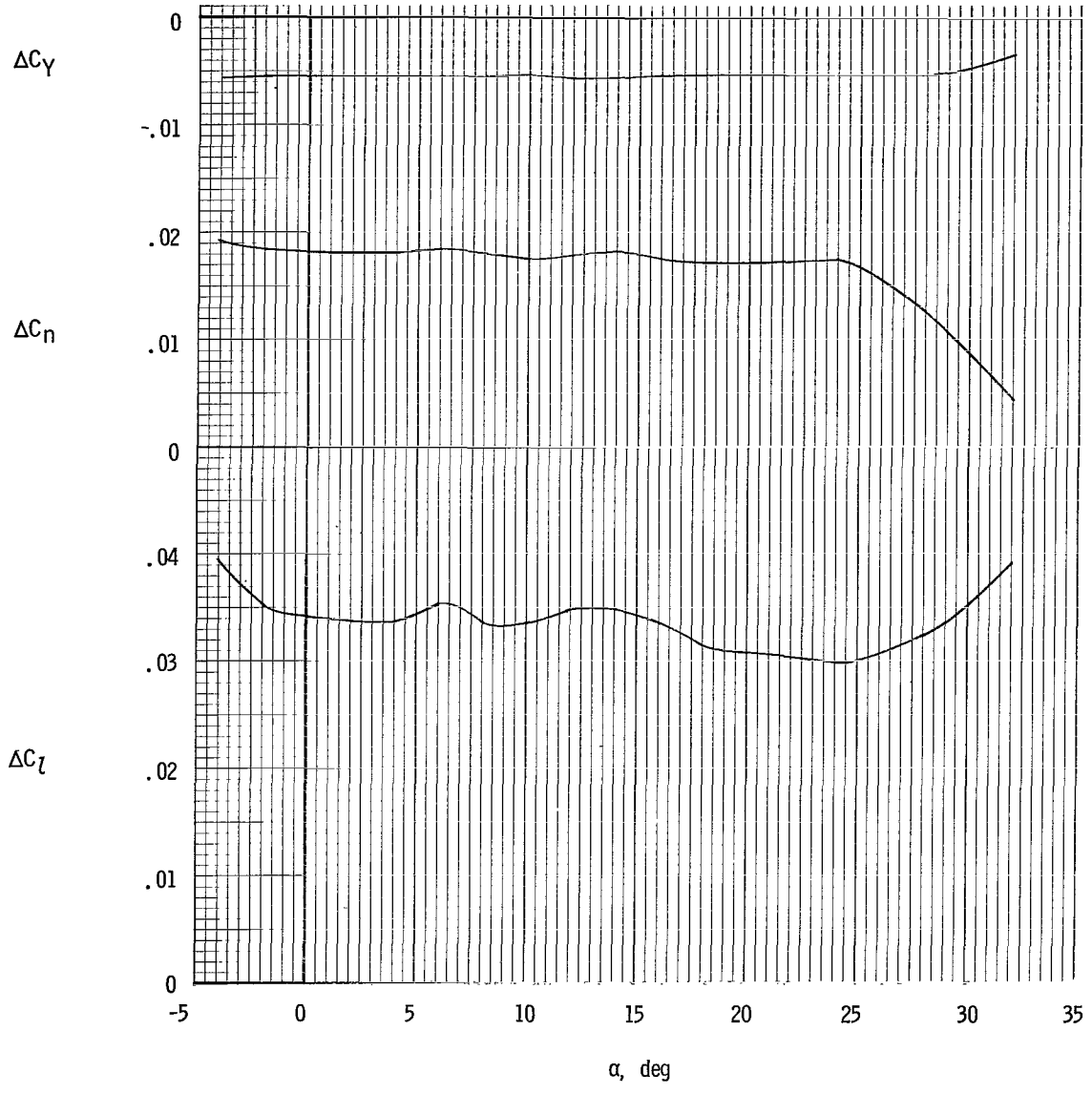

(b) Surfaces e_1, e_2, and e_3. $\delta_n = -40^0$; $\delta_a = 40^0$.

Figure 10.- Concluded.

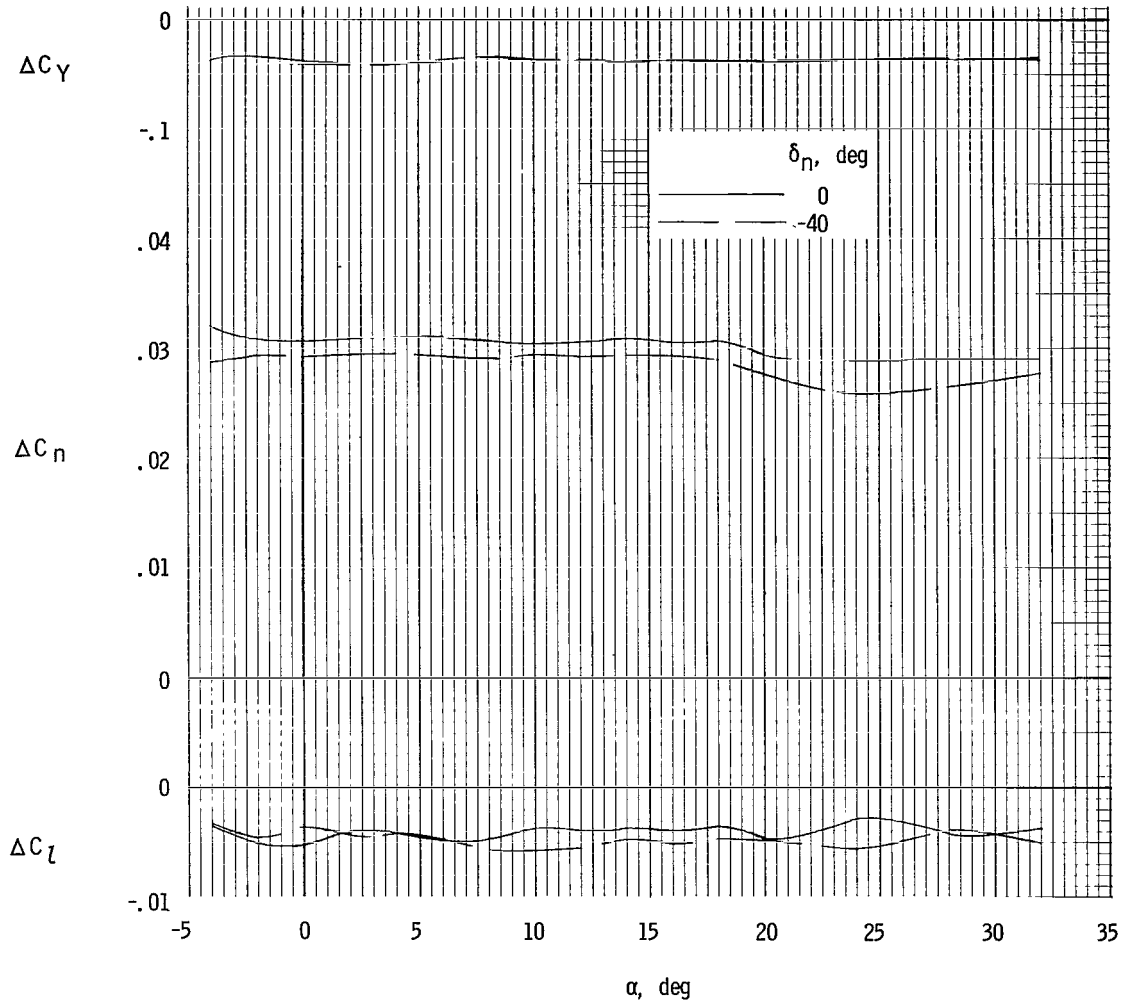

Figure 11.- Rudder control effectiveness of the model. $\delta_r = -28^0$.

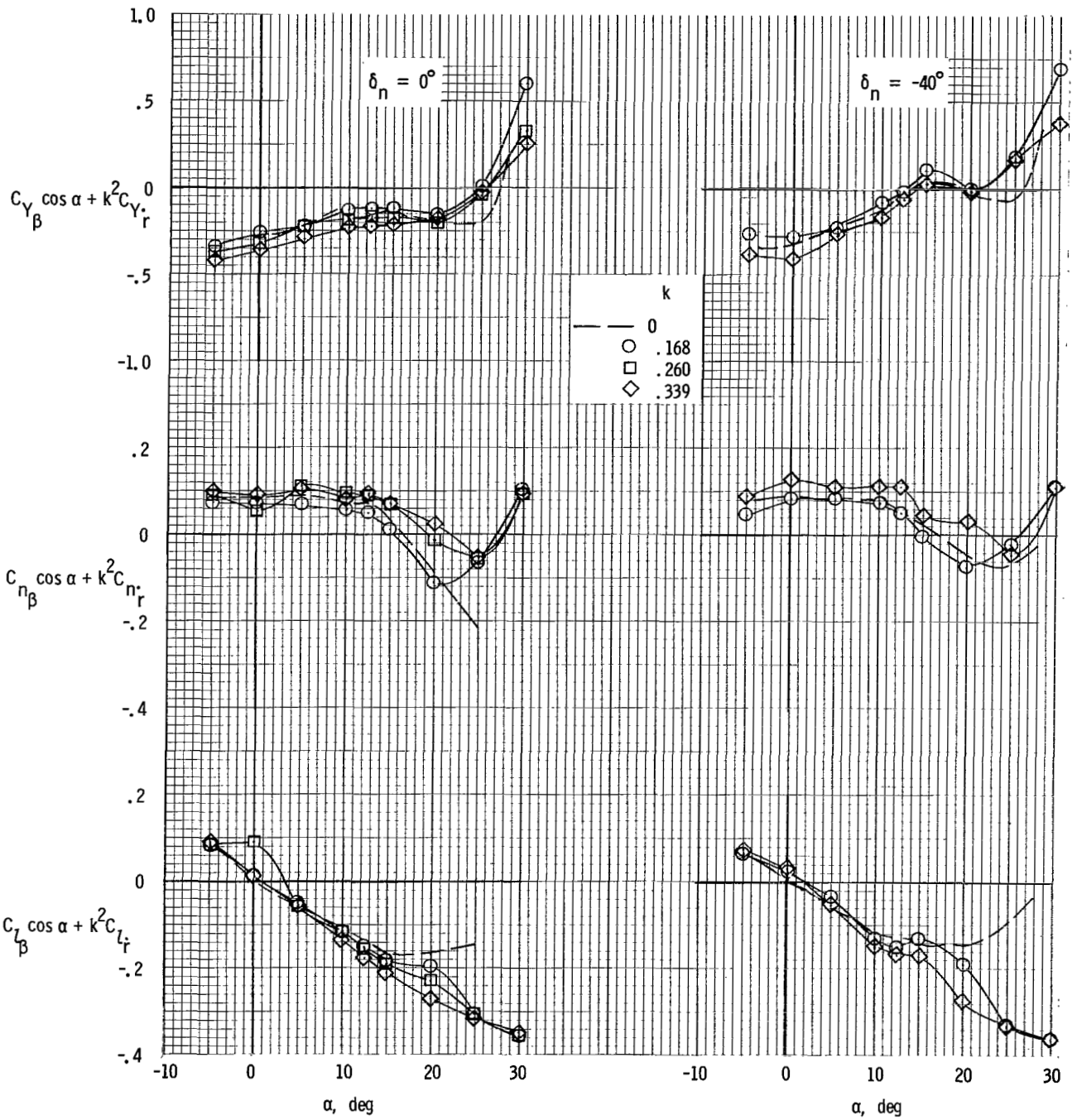

(a) In phase.

Figure 12.- Derivatives measured in yawing oscillation tests.

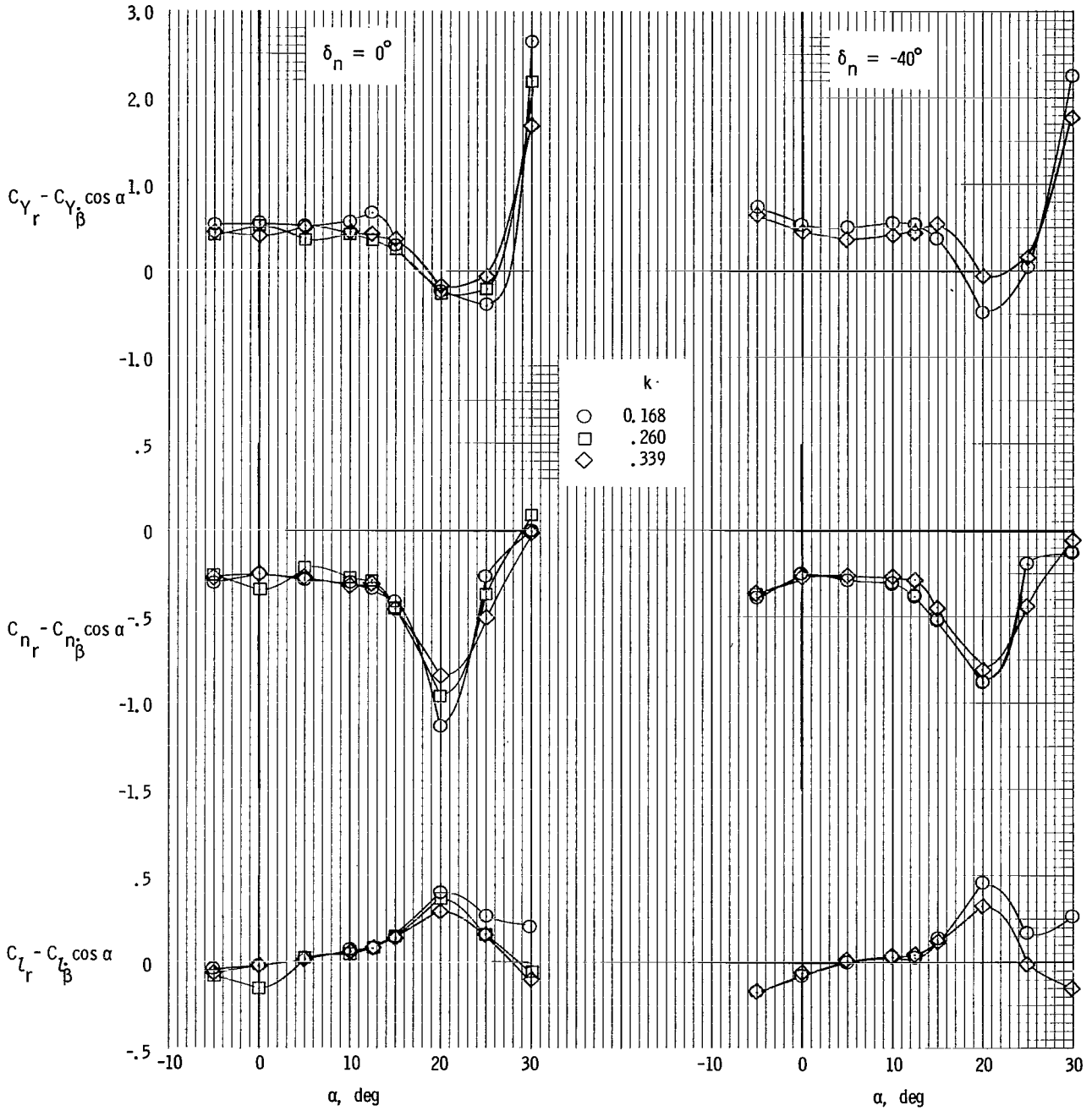

(b) Out of phase.

Figure 12.- Concluded.

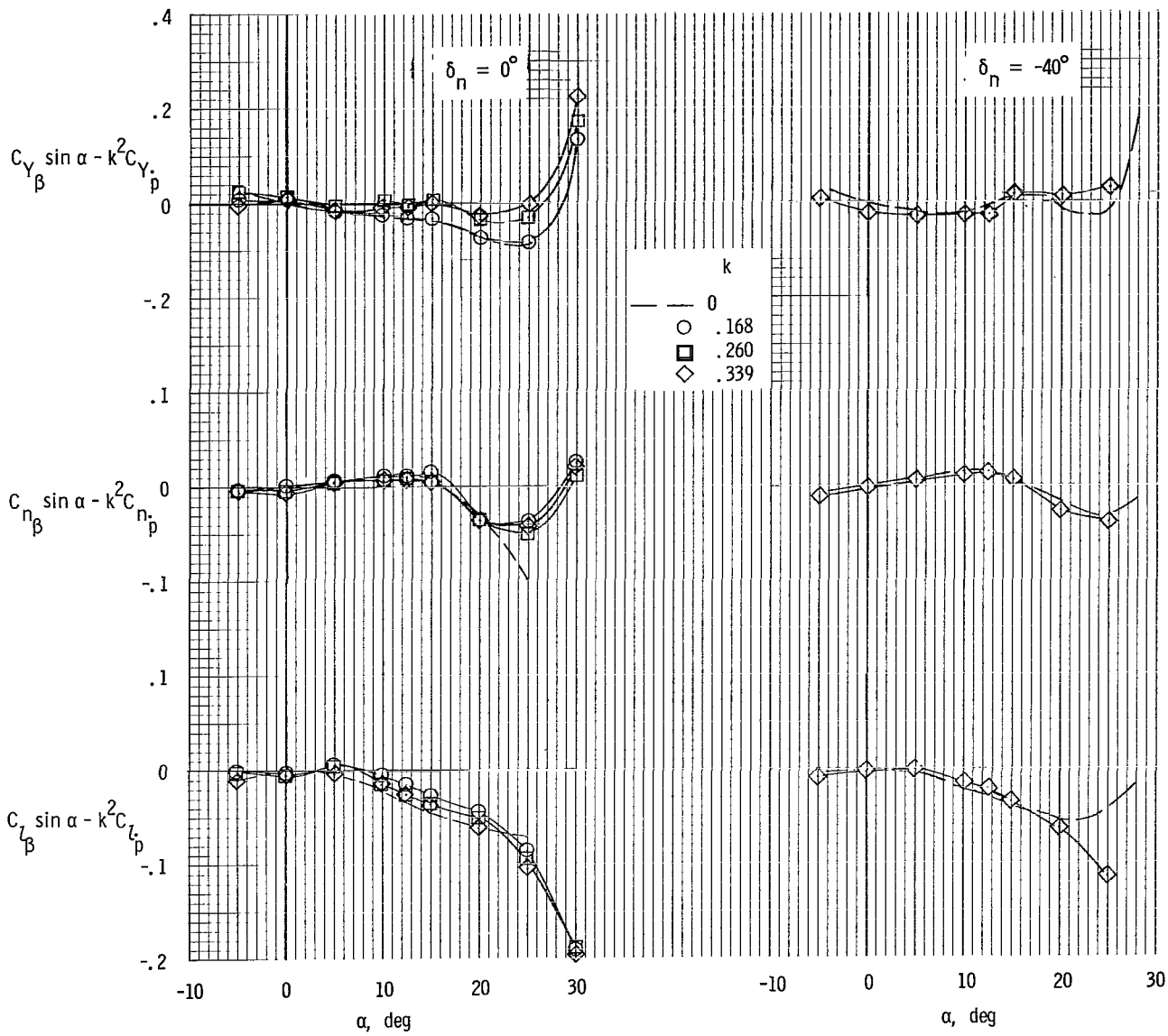

(a) In phase.

Figure 13.- Derivatives measured in rolling oscillation tests.

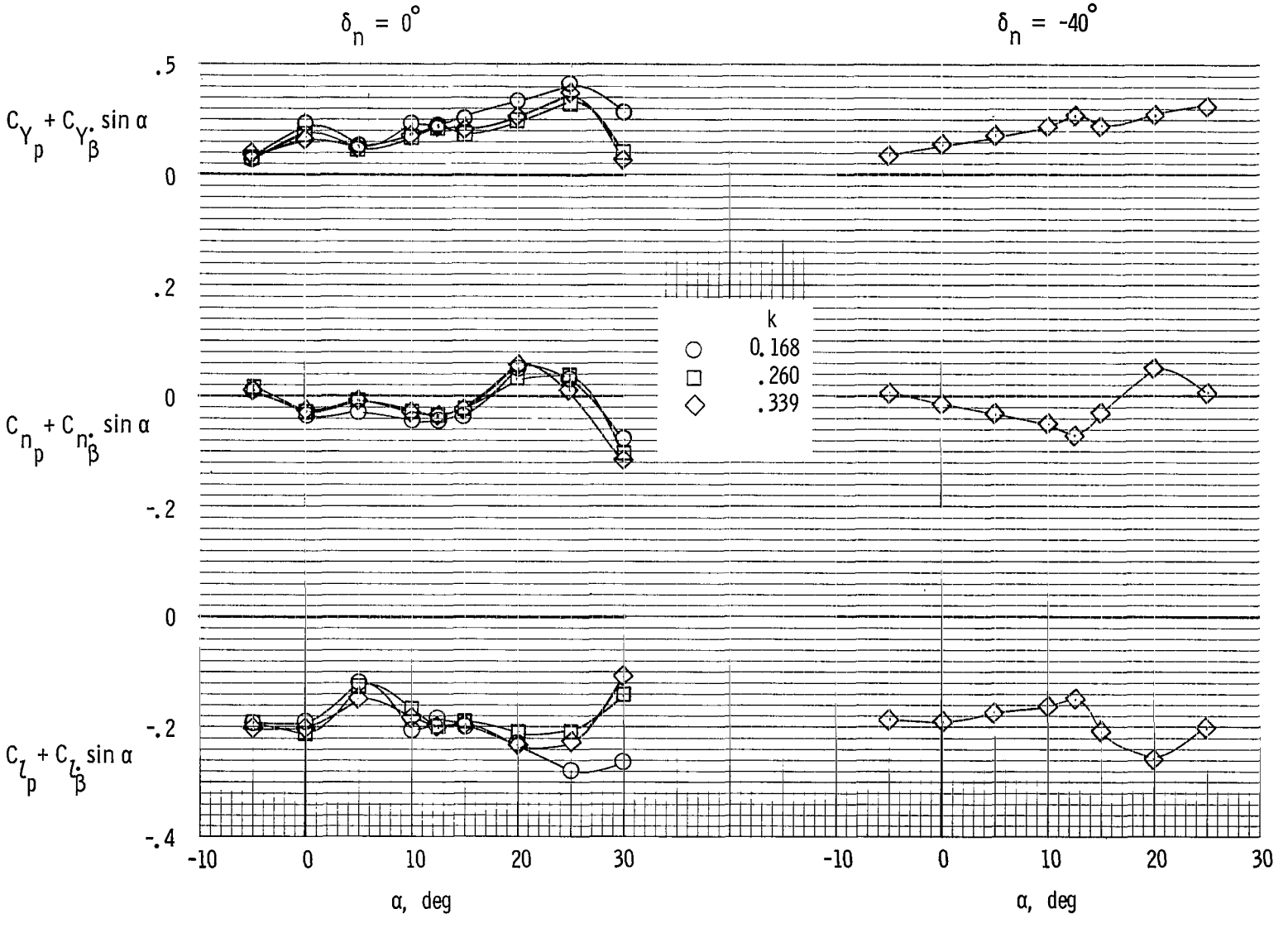

(b) Out of phase.

Figure 13.- Concluded.

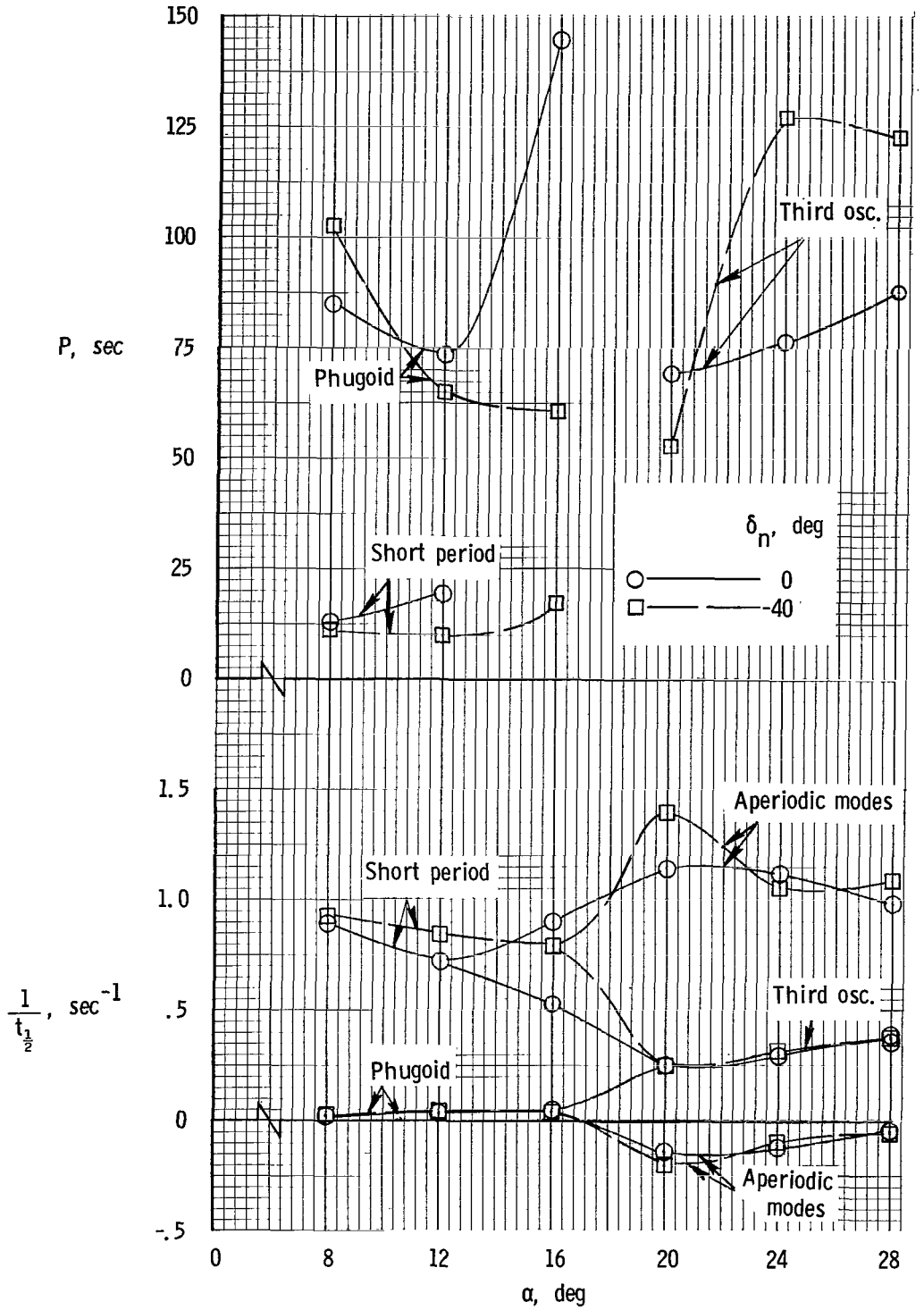

Figure 14.- Calculated longitudinal period and damping characteristics for the full-scale configuration. Calculations based on measured test data of present investigation.

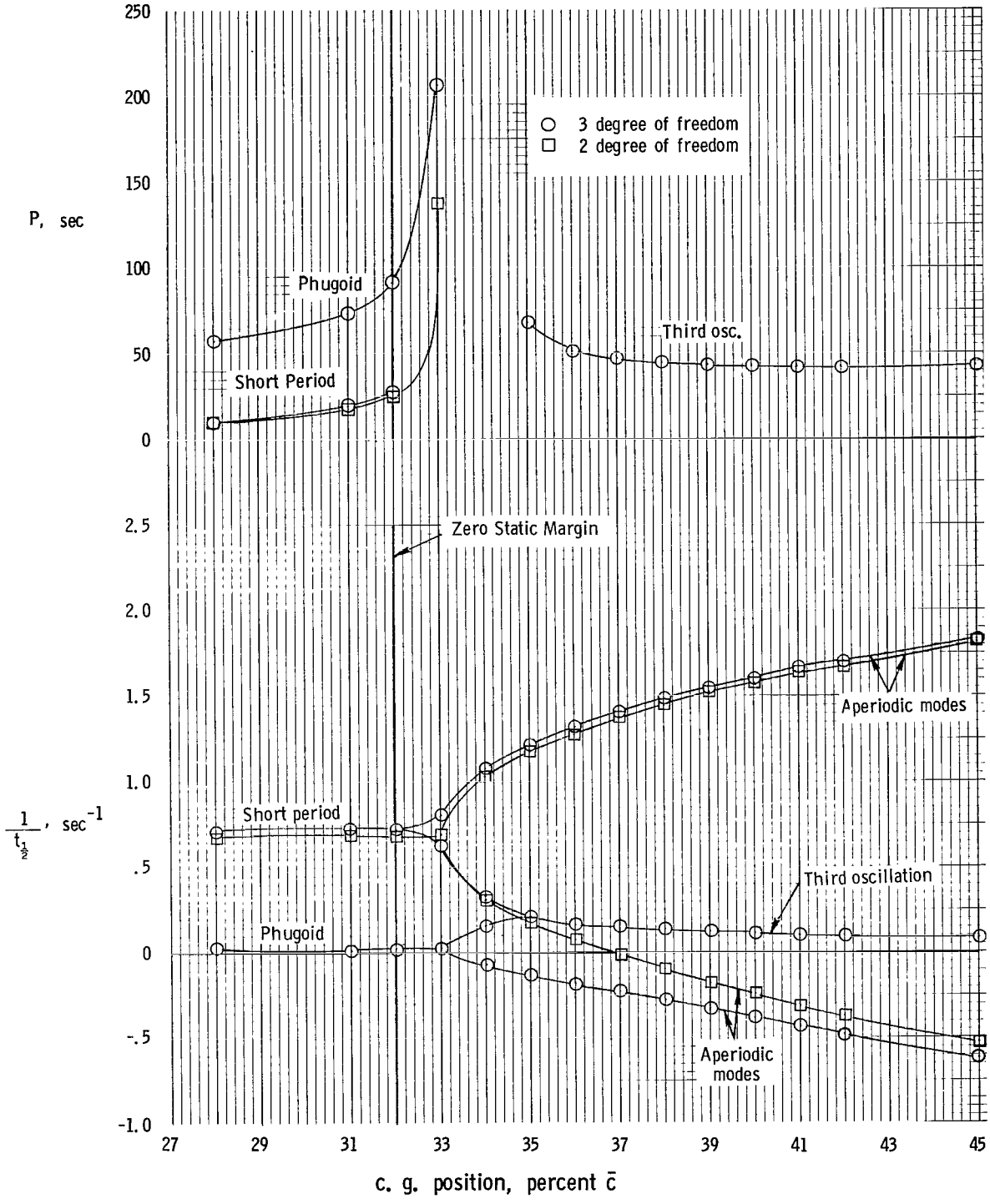

Figure 15.- Calculated longitudinal period and damping characteristics for full-scale configuration showing effect of center-of-gravity travel. Calculations based on measured test data of present investigation. $\delta_n = 0^0$; $\alpha = 12^0$.

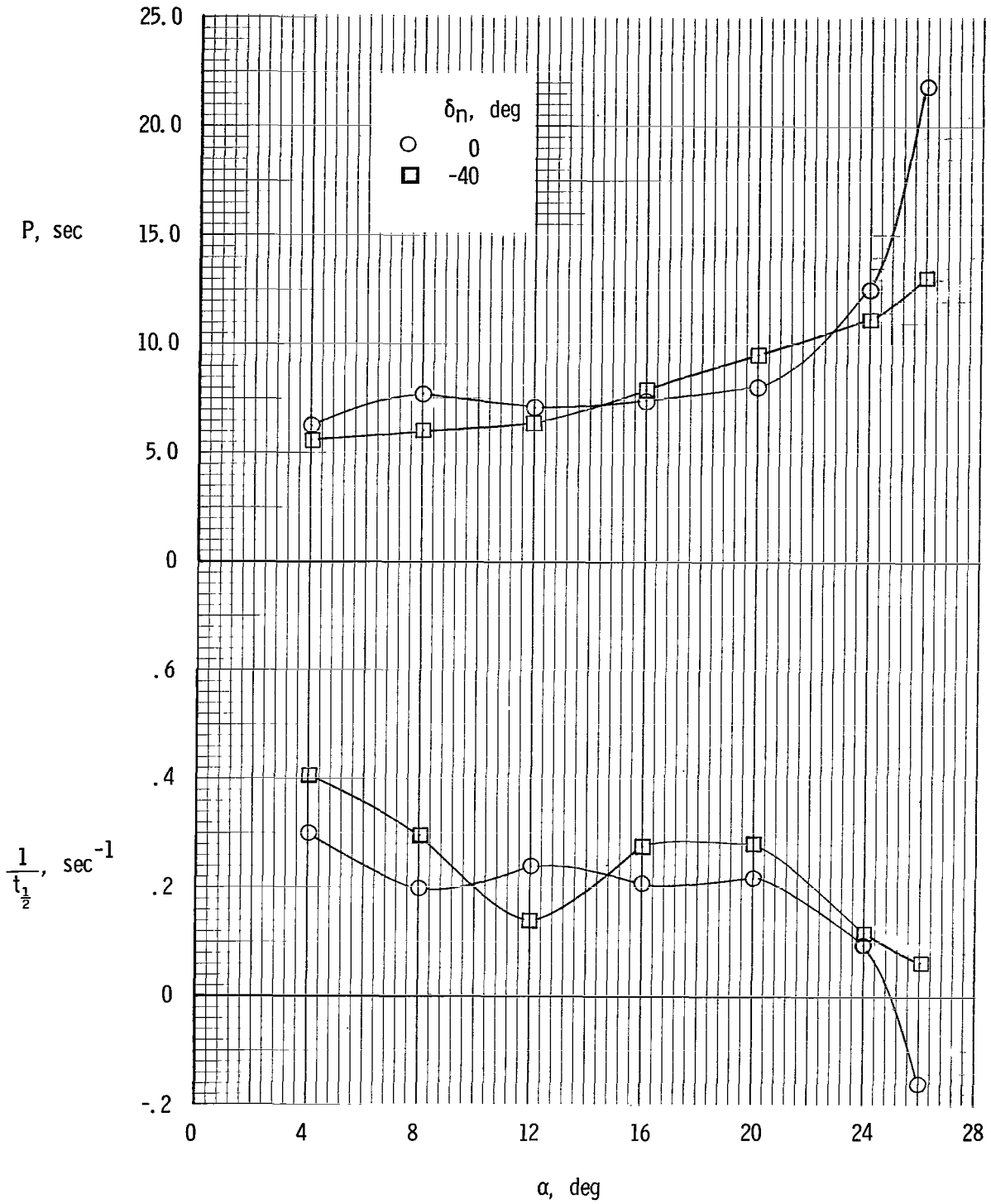

Figure 16.- Calculated period and damping characteristics for the full-scale configuration of Dutch roll oscillation. Calculations based on measured force-test data of present investigation.

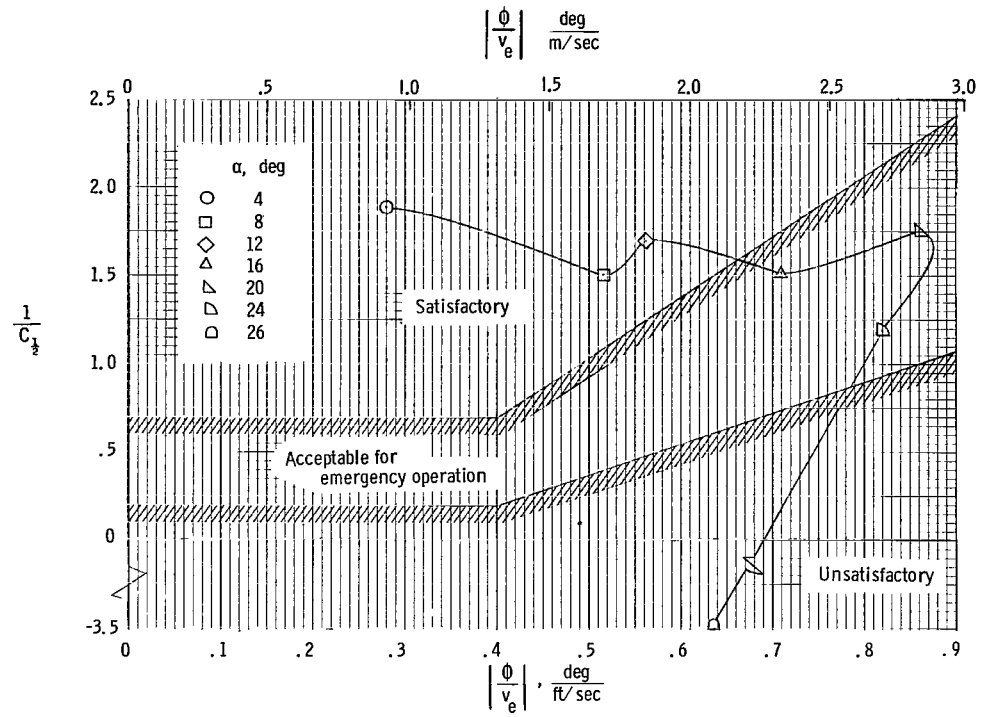

(a) $\delta_n = 0^o$.

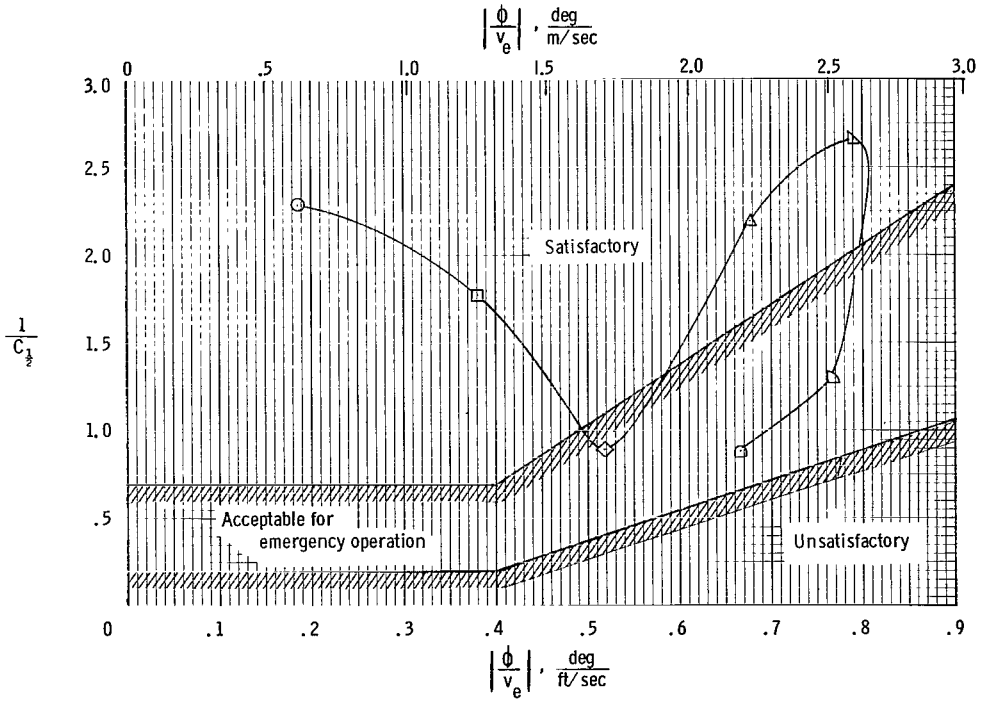

(b) $\delta_n = -40^o$.

Figure 17.- The lateral oscillatory characteristics of the model compared with military requirements for satisfactory aircraft handling qualities.

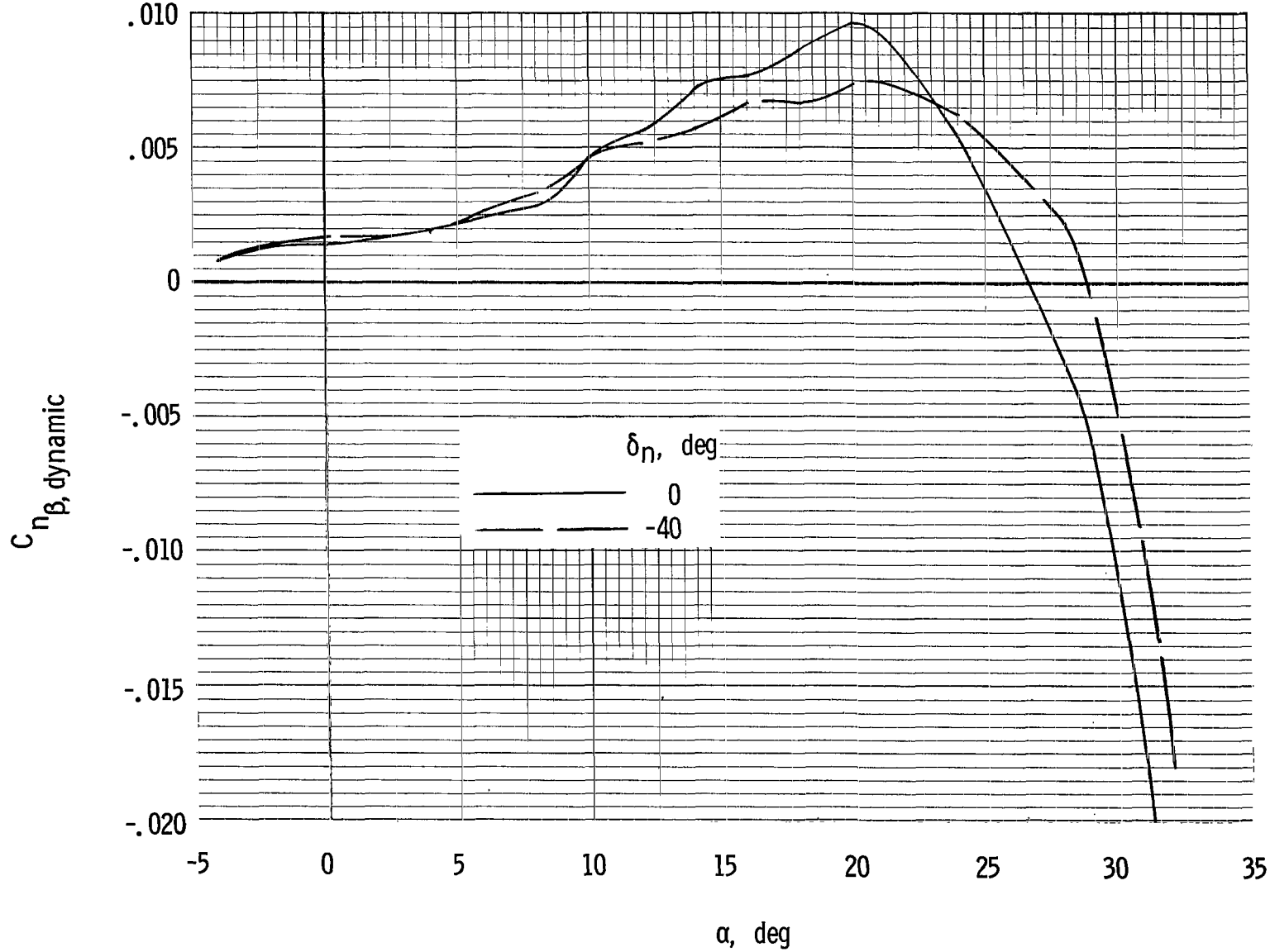

Figure 18.- Calculated values of $C_{n_{\beta,\text{dynamic}}}$.

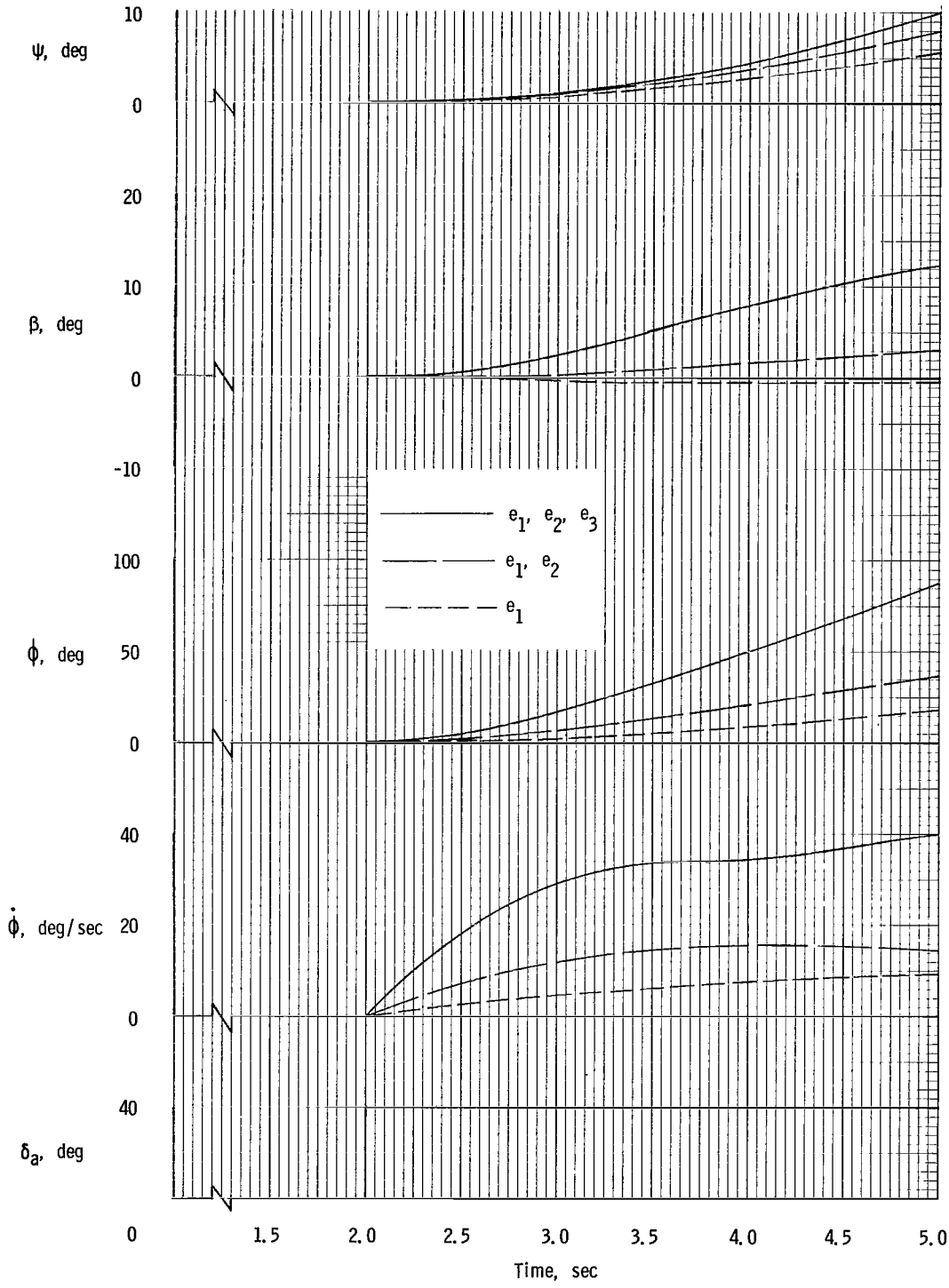

Figure 19.- Calculated full-scale roll control response (calculations based on measured force-test data of present investigation). $\alpha = 12^{0}$; $\delta_n = 0$.

National Aeronautics and Space Administration
WASHINGTON, D. C.

OFFICIAL BUSINESS

FIRST CLASS MAIL

POSTAGE AND FEES PAID
NATIONAL AERONAUTICS AND
SPACE ADMINISTRATION

06U 001 27 51 3DS 68059 00903
AIR FORCE WEAPONS LABORATORY/AFWL/
KIRTLAND AIR FORCE BASE, NEW MEXICO 87117

ATT MISS MADELINE F. CANOVA, CHIEF TECHNICA
LIBRARY /WLIL/

POSTMASTER: If Undeliverable (Section 158 Postal Manual) Do Not Return

"The aeronautical and space activities of the United States shall be conducted so as to contribute . . . to the expansion of human knowledge of phenomena in the atmosphere and space. The Administration shall provide for the widest practicable and appropriate dissemination of information concerning its activities and the results thereof."

—NATIONAL AERONAUTICS AND SPACE ACT OF 1958

NASA SCIENTIFIC AND TECHNICAL PUBLICATIONS

TECHNICAL REPORTS: Scientific and technical information considered important, complete, and a lasting contribution to existing knowledge.

TECHNICAL NOTES: Information less broad in scope but nevertheless of importance as a contribution to existing knowledge.

TECHNICAL MEMORANDUMS: Information receiving limited distribution because of preliminary data, security classification, or other reasons.

CONTRACTOR REPORTS: Scientific and technical information generated under a NASA contract or grant and considered an important contribution to existing knowledge.

TECHNICAL TRANSLATIONS: Information published in a foreign language considered to merit NASA distribution in English.

SPECIAL PUBLICATIONS: Information derived from or of value to NASA activities. Publications include conference proceedings, monographs, data compilations, handbooks, sourcebooks, and special bibliographies.

TECHNOLOGY UTILIZATION PUBLICATIONS: Information on technology used by NASA that may be of particular interest in commercial and other non-aerospace applications. Publications include Tech Briefs, Technology Utilization Reports and Notes, and Technology Surveys.

Details on the availability of these publications may be obtained from:

SCIENTIFIC AND TECHNICAL INFORMATION DIVISION

NATIONAL AERONAUTICS AND SPACE ADMINISTRATION

Washington, D.C. 20546